

White Papers on Materials for Photoelectrochemical Water Splitting

CONTENTS

III-V Semiconductor Systems for High-Efficiency Solar Water Splitting Applications

Todd Deutsch, Heli Wang, Zhebo Chen, Shane Ardo, Shu Hu, Mahendra Sunkara, Dan Esposito, Yat Li, Shannon Boettcher

I-III-VI₂ Copper Chalcopyrites for Photoelectrochemical Water Splitting

Jess Kaneshiro, Todd Deutsch, Nicolas Gaillard, Zhebo Chen, Alan Kleiman-Shwarsstein, Feng Zhu, Michael Weir

The Viability of Using Tungsten Oxide Based Compounds as a Photoelectrode for the Solar Production of Hydrogen

Nicolas Gaillard, Yat Li, Heli Wang

Molybdenum Disulfide for Photoelectrochemical Water Splitting

Z. Chen, J.D. Benck, T.F. Jaramillo

Engineered Ternary and Quaternary Oxide Minerals with Optimal Absorption Characteristics for Solar-Assisted Low-Cost Hydrogen Production

Nicolas Gaillard, Muhammad N. Huda

BiVO₄ as a Photoanode for Photoelectrical Water Splitting

Kyoung-Shin Choi, Roel van de Krol

Hematite as a Photoelectrode for Photochemical Hydrogen Production

Heli Wang, Isabell Thomann, Arnold J. Forman, Yat Li, Mahendra Sunkara, Moreno de Respinis

Photovoltage of α -Fe₂O₃

Shannon W. Boettcher, Arnold J. Forman, Muhammad N. Huda, Heli Wang

The Viability of using Amorphous Silicon Carbide (α -SiC) as a Photoelectrode for PEC Hydrogen Production

Jian Hu, Feng Zhu, Ilvyda Matulionis, Josh Gallon, Nicolas Gaillard, and Todd Deutsch

Appendix: Current Matching

Jian Hu, Feng Zhu, Ilvyda Matulionis, Josh Gallon, Nicolas Gaillard, and Todd Deutsch

Appendix: Energetic Mismatch

Heli Wang, Arnold J. Forman, Moreno de Respinis, Nicolas Gaillard, Shannon Boettcher

Appendix: Design and Characterization of Photoelectrodes from First Principles

Tadashi Ogitsu, Brandon Wood, Wooni Choi, Muhammad N. Huda, Su-Huai Wei

PEC White Papers: III-V Semiconductors for PEC

III-V semiconductor systems for high-efficiency solar water splitting applications

Todd Deutsch¹, Heli Wang¹, Zhebo Chen², Shane Ardo³, Shu Hu³, Mahendra Sunkara⁴, Dan Esposito⁵, Yat Li⁶, Shannon Boettcher⁷

¹National Renewable Energy Laboratory, ²Stanford University, ³California Institute of Technology, ⁴University of Louisville, ⁵National Institute of Standards and Technology, ⁶University of California-Santa Cruz, ⁷University of Oregon

Introduction

Semiconductors composed of group IIIA and VA elements, commonly referred to as III-V's, represent a material class that demonstrates unparalleled photovoltaic (PV) and photoelectrochemical (PEC) conversion efficiencies. The current 43.5% PV efficiency¹ and 12.4% PEC water splitting efficiency² records were set with III-V semiconductor materials. These high efficiencies are a result of direct transition optical band gaps and the ability to grow low-defect epitaxial films that have long charge carrier lifetimes and high mobilities. Because III-V's have composition-dependent band gaps well matched to the solar spectrum (1-2 eV), they allow for multijunction configurations that can exceed the Shockley-Queisser efficiency limit³ for single junction photovoltaics. Multijunction cells also generate higher voltages, making them suitable for water-splitting applications where potential differences in excess of 1.7 V are required under operating conditions.

Technical Challenges

1. Interfacial band edge mismatch

One technical barrier is that the valence band edge of most III-V's, at least the ones that absorb visible light, is pinned at a potential that is insufficient (too negative) to drive the water oxidation half reaction⁴. This barrier can be addressed by incorporating a tandem architecture, by coupling with a separate photoanode, or by creating a buried photoactive junction such that the solution-absorber interface energetics become less important^{2,5,6}. The first two of these strategies increase the oxidation potential of the hole through photoexcitation in a secondary space charge region in the bulk or at a counter electrode while the last uses an ohmic contact at the semiconductor-electrolyte interface to unpin the band edges.

2. Stability

Material stability in aqueous electrolyte is the greatest challenge preventing implementation of III-V's in commercial solar-hydrogen photoreactors. The III-V materials are generally susceptible to corrosion via oxidation of the semiconductor components into solvated ions in the electrolysis bath⁷. Operating the semiconductor as a photocathode can provide cathodic protection from oxidation due the reducing environment and can extend the lifetime of III-V's in contact with an electrolyte, but unprotected surfaces can only withstand a few days of continuous operation. Economical PEC production of hydrogen demands the semiconductor operate without a significant loss in performance for several

PEC White Papers: III-V Semiconductors for PEC

thousand hours, a formidable challenge considering the inherent instability of the III-V's at the electrolyte interface.

3. Cost-effective high-volume synthesis

Technical challenges relating to the synthesis of III-V based materials in a cost-effective manner is another key issue that must be addressed in order to commercialize III-V PEC photoreactors. III-V's are typically synthesized by metal organic chemical vapor deposition (MOCVD) or molecular beam epitaxy (MBE). MOCVD relies on highly toxic, pyrophoric, and expensive precursors. MBE is a slow ultra-high vacuum process. The multilayer device architectures and abrupt interfaces require these precision epitaxial deposition techniques, which utilize expensive single-crystal growth templates that are difficult to reuse. Therefore, although the active film thickness for III-Vs is typically 1-2 μm (due to the high absorption coefficient associated with a direct band gap), the growth substrate that the absorber resides on is typically several hundred μm -thick. The confluence of specialized batch synthesis and high substrate costs can make the finished semiconductor prohibitively expensive. Currently a 6" (182 cm^2) GaAs substrate suitable for epitaxy costs about \$180, making the substrate contribution alone about \$10,000/ m^2 . The highest PEC water-splitting efficiency was measured under 12 suns² demonstrating that III-V's can be used with moderate light concentration. A photoreactor design using moderate light concentration (10x) could thus require only about 1/10th the absorber material per reactor unit area, leading to material economy. Despite incurring additional balance of systems costs, including tracking systems, as well as the loss in the ability to utilize much of the diffuse solar irradiation, techno-economic analysis⁸ of a 10x concentrator reactor suggests that hydrogen would be commercially viable from a stable and efficient material with an absorber cost of \$150/ m^2 . Light emitting diode III-V synthesis has seen a dramatic reduction in semiconductor cost by maximizing the yield per batch through increased wafer size and multiple wafers per reactor.

There are a few techniques that exist that offer low-cost alternatives to MOCVD and MBE. Vapor-liquid-solid (VLS) growth mechanism allows for seeding of single-crystal semiconductor wires off arbitrary substrates. Usually, (111)-oriented single crystal substrates are used to grow vertically-aligned single crystal Si or GaAs wire arrays. Textured polycrystalline films with (111)-preferred orientation deposited on low-cost glass or flexible sheets can be used as growth templates for assembling aligned nanowire or microwire light absorbers^{9,10}. Another potential approach is to utilize nanowire to microwire arrays as substrates for growing thick epitaxial layers thus reducing the need for expensive, single crystal substrates¹¹. The wire geometry is more forgiving of strain from near-epitaxial growth in comparison to planar materials, and epitaxy is preferred for tandem device fabrication. The processes for nanowire array substrates are scalable for large areas; however, contacting a mat of randomly oriented nanowires can be nontrivial. Nanosphere lithography allows for wafer-scale synthesis of nanowires¹². Scaling-up of MOCVD process and large-scale nano-patterning techniques (e.g. nano-imprint lithography) is currently being pursued by the semiconductor manufacturing industry.

PEC White Papers: III-V Semiconductors for PEC

Research Status

The highest direct, unbiased solar photoelectrolysis efficiency was achieved using a tandem III-V semiconductor: a p-GaInP₂ PEC junction integrated with a p/n-GaAs photovoltaic converted illumination to hydrogen and oxygen at 12.4% solar to hydrogen (STH) efficiency². This measurement was made under 12x light intensity showing the viability of moderate concentration in these devices. After 20 hours, the short-circuit current density dropped from 120mA/cm² to 105 mA/cm² (10.8% STH) and although the entire surface continued to evolve gas bubbles, areas of localized damage were observed.

Recent results indicate that an improved efficiency can be obtained by using a more active oxygen evolution counter electrode. When RuO₂ was used instead of platinum black, the two-terminal J-V curve was shifted towards higher efficiencies. An efficiency under real-solar (outdoor) conditions of 16.3% was measured, but this was under a moderate bias¹³. The most recent iteration of the tandem cells did not match the performance of those used to establish the 12.4% unbiased efficiency benchmark due to current difficulties in achieving reproducible synthesis, a problem that must be addressed prior to scale-up. It is likely that the short-circuit efficiency of the original materials would have been greater had RuO₂ been used.

Two efforts to stabilize III-V's using nitrides have had moderate success. The inclusion of the nitride in the bulk of GaP demonstrated an ability to reduce the corrosion on the III-V surface^{14,15}, however, the nitride also led to a significant loss in photoconversion efficiency. A nitrogen ion implantation treatment on p-GaInP₂ surfaces (without a buried p/n GaAs junction) has been extremely successful in nearly eliminating corrosion by generating a surface nitride layer. One nitride treated sample exhibited no detectable damage after 115-hours of passing a constant -10mA/cm² photocurrent, the equivalent to 12.3% solar-to-hydrogen conversion¹⁶. The nitride treatment did lead to an approximate 5% relative loss in (light-limited reverse bias) photoconversion ability, but this minimal loss could be tolerated by a 12% STH cell and still exceed the 10% benchmark.

Approaches

Research on III-Vs for PEC applications focuses primarily on utilizing proven high-efficiency configurations and engineering a stabilized surface. Protection of the surface can be accomplished through inclusion of a stabilizing agent throughout the bulk during synthesis, such as the incorporation of a dilute nitride. Other areas of research aim at surface or near-surface treatments that can chemically protect the interface while maintaining a low interface defect density and fast charge transfer to the surface attached electrocatalyst. Some surface treatments are in the form of coatings (oxides via atomic layer deposition, polymers, metal overcoats, catalysts). Other treatments are aimed at changing the near surface chemistry through application of a plasma, via electrochemical means, or by ion-implantation.

Research on III-V synthesis, not necessarily for only PEC applications, has focused on two key areas; reusing the expensive substrate or eliminating it entirely. Synthesis routes that maximize the substrate utility are epitaxial lift-off^{17,18} (ELO)

PEC White Papers: III-V Semiconductors for PEC

and inverted metamorphic multijunction¹⁹ (IMM). Both of these approaches are currently being exploited by industry (Alta Devices, RFMD). Another approach, close spaced vapor transport (CSVST), seeks to eliminate the substrate and the costly metal organic precursors. Dopant diffusion at the high temperatures required for CSVST could compromise abrupt junctions in certain cases and prevent CSVST from providing complex multilayer configurations. However, high efficiency dual-photoelectrode systems have been demonstrated that use simple combinations of a p-type photocathode and n-type photoanode⁵. The fast growth rate of high-quality, single conductivity type materials makes CSVST an attractive route to high volume production of dual absorber systems²⁰, especially if growth on low-cost substrates can be accomplished.

Another approach is based on modification of the wide band gap (3.4eV) semiconductor GaN, a stable III-V material that has band edges that encompass the water splitting half-reaction potentials. This route uses the indium content in a pure nitride alloy $\text{In}_x\text{Ga}_{1-x}\text{N}$ as a lever to tune the band gap and band edge positions. InN and GaN have a lattice mismatch of close to 12% making synthesis high indium content films challenging via conventional (high temperature) methods due to strain induced effects²¹. Low temperature epitaxial routes that use energetic atoms in lieu of plasma have overcome this miscibility gap^{22,23}. GaN has better corrosion resistance than other metal nitrides (e.g., Ta_3N_5) and phosphides (e.g., GaP), but the long term stability is still not comparable to metal oxides²⁴⁻²⁶. Stabilizing $\text{In}_x\text{Ga}_{1-x}\text{N}$ photoelectrodes is a key issue that remains to be solved.

Research on III-V materials also includes synthesizing alloys of GaN using small amounts of antimony (<5 at%) to obtain alloys with band gaps below 2.4 eV²⁷. These alloys with dilute antimony compositions have been predicted to straddle hydrogen and oxygen evolution reactions.

References

1. Green, M. A., Emery, K., Hishikawa, Y., Warta, W. & Dunlop, E. D. Solar cell efficiency tables (version 39). *Progress in Photovoltaics: Research and Applications* **20**, 12–20 (2012).
2. Khaselev, O. & Turner, J. A monolithic photovoltaic-photoelectrochemical device for hydrogen production via water splitting. *Science (New York, N.Y.)* **280**, 425–7 (1998).
3. Shockley, W. & Queisser, H. J. Detailed Balance Limit of Efficiency of p-n Junction Solar Cells. *Journal of Applied Physics* **32**, 510–519 (1961).
4. Kocha, S. S., Turner, J. A. & Nozik, A. J. Study of the Schottky barrier and determination of the energetic positions of band edges at the n- and p-type gallium indium phosphide electrode | electrolyte interface. *Journal of Electroanalytical Chemistry* **367**, 27–30 (1994).

PEC White Papers: III-V Semiconductors for PEC

5. Kainthla, R. C., Zelenay, B. & Bockris, J. O. M. Significant Efficiency Increase in Self-Driven Photoelectrochemical Cell for Water Photoelectrolysis. *Journal of The Electrochemical Society* **134**, 841 (1987).
6. Boettcher, S. W. *et al.* Energy-conversion properties of vapor-liquid-solid-grown silicon wire-array photocathodes. *Science (New York, N.Y.)* **327**, 185–7 (2010).
7. Khaselev, O. & Turner, J. A. Electrochemical Stability of p-GaInP₂ in Aqueous Electrolytes Toward Photoelectrochemical Water Splitting. *Journal of The Electrochemical Society* **145**, 3335–3339 (1998).
8. James, B. D., Baum, G. N., Perez, J. & Baum, K. N. *Technoeconomic Analysis of Photoelectrochemical (PEC) Hydrogen Production*. 1–127 (2009).at <http://www1.eere.energy.gov/hydrogenandfuelcells/pdfs/pec_technoeconomic_analysis.pdf>
9. Chuang, L. C. *et al.* Critical diameter for III-V nanowires grown on lattice-mismatched substrates. *Applied Physics Letters* **90**, 043115 (2007).
10. Tomioka, K., Kobayashi, Y., Motohisa, J., Hara, S. & Fukui, T. Selective-area growth of vertically aligned GaAs and GaAs/AlGaAs core-shell nanowires on Si(111) substrate. *Nanotechnology* **20**, 145302 (2009).
11. Pendyala, C. *et al.* Nanowires as semi-rigid substrates for growth of thick, In(x)Ga(1-x)N (x > 0.4) epi-layers without phase segregation for photoelectrochemical water splitting. *Nanoscale* **4**, 6269–75 (2012).
12. Madaria, A. R. *et al.* Toward optimized light utilization in nanowire arrays using scalable nanosphere lithography and selected area growth. *Nano letters* **12**, 2839–45 (2012).
13. Turner, J. A. & Deutsch, T. G. Semiconductor Materials for Photoelectrolysis. *Proceedings of the 2011 U.S. Department of Energy Hydrogen and Fuel Cells Program and Vehicle Technologies Program Annual Merit Review and Peer Evaluation Meeting* (2011).
14. Deutsch, T. G., Head, J. L. & Turner, J. A. Photoelectrochemical Characterization and Durability Analysis of GaInPN Epilayers. *Journal of The Electrochemical Society* **155**, B903 (2008).
15. Deutsch, T. G., Koval, C. A. & Turner, J. A. III-V nitride epilayers for photoelectrochemical water splitting: GaPN and GaAsPN. *The Journal of Physical Chemistry B* **110**, 25297–307 (2006).

PEC White Papers: III-V Semiconductors for PEC

16. Deutsch, T. G. & Turner, J. A. Semiconductor Materials for Photoelectrolysis. *Proceedings of the 2012 U.S. Department of Energy Hydrogen and Fuel Cells Program and Vehicle Technologies Program Annual Merit Review and Peer Evaluation Meeting* (2012).
17. Yoon, J. *et al.* GaAs photovoltaics and optoelectronics using releasable multilayer epitaxial assemblies. *Nature* **465**, 329–33 (2010).
18. Schermer, J. J. *et al.* Epitaxial Lift-Off for large area thin film III/V devices. *Physica Status Solidi (a)* **202**, 501–508 (2005).
19. Geisz, J. F. *et al.* 40.8% Efficient Inverted Triple-Junction Solar Cell With Two Independently Metamorphic Junctions. *Applied Physics Letters* **93**, 123505 (2008).
20. Ritenour, A. J., Cramer, R. C., Levinrad, S. & Boettcher, S. W. Efficient n-GaAs Photoelectrodes Grown by Close-Spaced Vapor Transport from a Solid Source. *ACS Applied Materials & Interfaces* **4**, 69–73 (2012).
21. Moses, P. G. & Van de Walle, C. G. Band bowing and band alignment in InGaN alloys. *Applied Physics Letters* **96**, 021908 (2010).
22. Williamson, T. L., Williams, J. J., Hubbard, J. C. D. & Hoffbauer, M. A. High In content In_xGa_{1-x}N grown by energetic neutral atom beam lithography and epitaxy under slightly N-rich conditions. *Journal of Vacuum Science & Technology B: Microelectronics and Nanometer Structures* **29**, 03C132 (2011).
23. Williamson, T. L., Salazar, A. L., Williams, J. J. & Hoffbauer, M. a. Improvements in the compositional uniformity of In-rich In_xGa_{1-x}N films grown at low temperatures by ENABLE. *Physica Status Solidi (C)* **8**, 2098–2100 (2011).
24. Li, J., Lin, J. Y. & Jiang, H. X. Direct hydrogen gas generation by using InGaN epilayers as working electrodes. *Applied Physics Letters* **93**, 162107 (2008).
25. Ryu, S.-W., Zhang, Y., Leung, B., Yerino, C. & Han, J. Improved photoelectrochemical water splitting efficiency of nanoporous GaN photoanode. *Semiconductor Science and Technology* **27**, 015014 (2012).
26. Waki, I. *et al.* Direct water photoelectrolysis with patterned n-GaN. *Applied Physics Letters* **91**, 093519 (2007).
27. Sheetz, R. M. *et al.* Visible light absorption and large band gap bowing in dilute alloys of gallium nitride with antimony. *Physical Review Letters* **84**, 075304 (2011).

PEC White Papers: I-III-VI₂ for PEC Hydrogen Production

I-III-VI₂ Copper Chalcopyrites

Primary Authors & Affiliations:

Jess Kaneshiro (HNEI), Todd Deutsch (NREL), Nicolas Gaillard (HNEI), Zhebo Chen (Stanford U.), Alan Kleiman-Shwarsstein (Solopower), Feng Zhu (MVSsystems), Michael Weir (UNLV)

Introduction:

The I-III-VI₂ alloyed semiconductor class, championed in the photovoltaic (PV) scientific field by Cu(In_xGa_{1-x})Se₂ (often abbreviated “CIGS”)¹, incorporates a wide range of materials that are useful in solar energy conversion. Within this material class, bandgaps between 1.0eV and 2.43eV can be obtained by varying the alloy ratios in each elemental group². Of most interest for photoelectrochemical (PEC) water-splitting is the higher-bandgap members of this class, such as CuGaSe₂ with a bandgap of 1.65eV which has served generally as the baseline material for this application.

The variable bandgap of the copper chalcopyrite compounds has been studied extensively, most often for PV applications, making this material class particularly attractive for the development of PEC materials and systems by utilizing the very rich existing knowledge base^{1,2}. The very high Cu(InGa)Se₂ PV conversion efficiency of 20.3% (Nov. 2011) with lower-bandgap material is made possible by the strong optical absorption due to a direct bandgap, exceptional carrier transport properties, and compositional tunability enabling highly beneficial bandgap grading³. These traits are just as important for a PEC device and are, for the most part, maintained in the higher-bandgap materials like CuGaSe₂. Despite the existing knowledge base, significant work is needed to tune the material properties (e.g. bandgap, band edge alignment, and corrosion resistance; see White Paper Appendix) for PEC applications. Previous work has demonstrated photocurrents as high as 20mA/cm² in a PEC application, stability in very highly acidic electrolytes, and durability up to 420 hours⁴. It is worth mentioning that any CIGSe-based PEC technologies would rely on existing fabrication techniques already implemented for CIGSe PV technologies, allowing for the rapid deployment of PEC devices when a suitable material is developed.

Because materials viable for PEC devices have high bandgaps, much of the visible solar spectrum is not absorbed. This offers the opportunity to harvest the unabsorbed photons with underlying PV cells of smaller bandgaps resulting in multi-junction devices that can more effectively utilize incident light⁴. Multi-junction devices are electrically connected in series, resulting in a summation of voltages to counteract typically insufficient band edge alignment and kinetic overpotentials of the water-splitting reactions. Multi-junction absorbers have been utilized to achieve world record efficiencies in both PV⁵ and PEC⁶ devices utilizing the III-V material class, and are the optimal configuration in the development of most planar PEC water-splitting devices. This is particularly convenient for alloyed semiconductors like the I-III-VI₂ material class because the ability to engineer the bandgaps by alloy compositions permit tuning to optimize absorption via multi-layers within the same material class.

Technical Challenges:

The research philosophy in this material class has so far aimed to take an optimized material (Cu(InGa)Se₂), proven to have excellent optoelectronic properties in the PV

PEC White Papers: I-III-VI₂ for PEC Hydrogen Production

field, and repurpose it for the requirements of water-splitting. The first requirement is a high bandgap of *at least* 1.23eV, and preferably much higher in the 1.6-2.1eV range^{4,7}. By removing In from optimized PV devices resulting in CuGaSe₂, the bandgap is raised to a modest 1.65eV, which can, in an appropriate configuration, be used to split water. CuGaSe₂ thus serves as the baseline material for this material class. Its chemical simplicity, ease of fabrication, and close relation to commercial PV Cu(InGa)Se₂ has resulted in very robust fabrication of high-quality cells, and performance and durability have proven to be exceptional^{4,8,9,10}.

With the increase of Ga, however, the bandgap is expanded by a rise in the conduction band while the valence band remains misaligned with respect to the oxygen evolution potential⁴. This occurs because the valence band energy is dominated by the Cu-3d to Se-4p orbital bond, which is unaffected by the group-III alloy content (In,Ga)¹¹. Furthermore, CuGaSe₂ is subjected to the “doping pinning rule”, common in highly-doped semiconductors, wherein the Fermi level is pinned at a certain level interrupting the band bending vital to photovoltage production¹². This doping pinning precludes the formation of a surface inversion layer that is very highly relied upon in Cu(InGa)Se₂ PV devices, resulting in a sub-proportional increase in open circuit voltages as bandgaps are raised with an increase in the Ga/(In+Ga) ratio^{11,13}. This effect is also evident in PEC devices where CuGaSe₂ exhibits very low photovoltage than would be expected for its bandgap, and therefore requires a very high voltage bias (presumably provided by light-harvesting PV cells) to split water.

Therefore (with the design philosophy of using CuGaSe₂ as a baseline material), the largest barrier in the I-III-VI₂ material class is overcoming the excessive voltage requirements originating from the misaligned valence band edge. Because the valence band energy is dominated by the I-VI bond (Cu-Se in the base case), it is the Cu and/or Se content that must be modified by, for example, replacing some Cu with Ag or Se with S. While both of which will raise the bandgap, the Se/S substitution may not significantly change the valence band maximum required to improve the band edge alignment¹⁴.

Research Status:

Band-edge misalignment in copper chalcopyrite films analyzed up until now makes unassisted water splitting impossible, and necessitates an external applied bias. While other device structures have been utilized, a monolithic stack of PEC and PV cells creating a hybrid photoelectrode (HPE) is the ultimate goal. At 1.65eV, typical 1 μ m-thick CuGaSe₂ cells are at the low end of optimum bandgap range (1.6-2.1eV), and do not pass sufficient light to underlying PV cells to provide enough voltage biasing. Recall that the band-edge misalignment in CuGaSe₂ results in a very high required voltage bias.

For this reason, alternative device designs were explored to utilize the very high photocurrents of optimized CuGaSe₂ of as high as 20mA/cm² by leveraging it towards photovoltage production. The resultant co-planar hybrid PV/PEC device employs 3 PV devices in a planar configuration next to a CuGaSe₂ PEC device. Because the devices are side-by-side, the total device area is the summation of the constituent devices. This is how the high current density of CuGaSe₂ is sacrificed to liberate real estate for PV devices to produce the voltage bias. Load-line analysis was used to determine the optimal ratio of PV/PEC areas and the resulting standalone device was tested outdoors producing 3.53mA/cm² at AM1.5G illumination, equivalent to a 4.35% solar-to-hydrogen (STH)

PEC White Papers: I-III-VI₂ for PEC Hydrogen Production

conversion efficiency⁴. Low-cost a-Si PV devices provided by MVSystems were utilized in this scheme, representing a relatively cheap solution to water-splitting. With 4 junctions, however, this device serves more as a proof-of-concept, described more in the following section, and would not by itself be a very practical device to split water because it operates at a relatively high voltage around 1.6V (2-terminal); a result of the unfavorably aligned band edges⁴.

CuGaSe₂, along with possessing high photocurrents, also benefits from excellent durability in very highly concentrated electrolytes. Higher ionic concentrations in the electrolyte provide better ionic conductivity, resulting in lower series resistance losses improving the “fill factor”, analogous to the term applied to J-V curves in PV technology. In 1M H₂SO₄ under AM1.5G illumination and biased to produce 4mA/cm² (the current density indicative of 5%STH efficiency), CuGaSe₂ has thus far demonstrated 420 hours of continuous operation before significant degradation of performance.

Approaches:

Having four coplanar junctions is not very practical as the high current is split across a larger absorption area, resulting in a lower overall device current density. A coplanar configuration also does not benefit from spectrum splitting, which more efficiently uses the potential of incident photons resulting in better voltage characteristics. This demonstration was valuable, however, as a starting point for device design advancement. Although CuGaSe₂ is currently unsuited for monolithic device integration, the coplanar device offers a proof-of-concept that I-III-VI₂ materials can be used in a PEC device that only uses light to split water. By showing that this device can achieve 4.35% STH with economical a-Si PV cells, extended simulation shows that burying just one PV cell can result in efficiencies upwards of 5% STH by reducing the area-division and increasing useable current density. As *material advancements* are achieved in the future, they can be inserted into this device design pathway to grasp both the full potential and the material performance goals that must be met to proceed further towards a monolithic device where all PV cells are buried.

The importance of material advancements is specifically highlighted by the need to address the valence band misalignment dominated by the I-VI bonds. It has already been theorized and demonstrated that the substitution of all or some of the selenium with sulfur (VI-elements) can increase the bandgap in copper chalcopyrites, and furthermore, sulfurization can lower the valence band placing it closer to the water oxidation potential^{2,15,16}. Material engineering can also be accomplished by manipulating the group I elements; partial replacement of Cu with Ag can slightly raise the bandgap as well as decrease the intrinsic p-type doping density. This may allow the formation of the surface inversion layer, aiding photovoltage development¹⁷.

Another potential research area is the use of Cu₂ZnSnS₄ (CZTS) and related materials for PEC. This material is technically a I₂-II-IV-VI₄ and effectively exchanges the group III atom (In, Ga) for 50% group II (Zn) and 50% group IV (Sn). CZTS is increasing in interest to the PV community because of the use of more abundant and sustainable elements¹⁸. CZTS is natively a p-type semiconductor with a bandgap of ~1.5 eV. However, the same elemental substitution approach from CIGS (e.g. Ag for Cu, Se for S) applies to CZTS and has been used to improve the solar conversion efficiency¹⁹. Only a

PEC White Papers: I-III-VI₂ for PEC Hydrogen Production

few reports of CZTS for PEC applications are available, leaving open the possibility of adapting this material to water splitting²⁰⁻²⁴.

Surface catalysis is another method of device enhancement being investigated to improve reaction kinetics. Progress with Pt and Ru nanoparticle treatments have shown increased performance, but lower cost solutions would be preferred.

-
- ¹ I. Repins, M.A. Contreras, B. Egaas, C. DeHart, J. Scharf, C.L. Perkins, B. To, R. Noufi, *Prog. Photovolt. Res. Appl.* **16** (2008) 235.
 - ² M. Bär, W. Bohne, J. Röhrich, E. Strub, S. Lindner, M.C. Lux-Steiner, Ch.-H. Fischer, *J. Appl. Phys.* **96** (2004) 3857.
 - ³ P. Jackson, D. Hariskos, E. Lotter, S. Paetel, R. Wuerz, R. Menner, W. Wischmann, M. Powalla, *Prog. Photovolt. Res. Appl.* **19** (2011) 894.
 - ⁴ J. Kaneshiro, Dissertation Thesis, University of Hawai'i at Mānoa, **2012**.
 - ⁵ S. Wojtczuk, P. Chiu, X. Zhang, D. Derkacs, C. Harris, D. Pulver and M. Timmons, *Photovoltaics Specialists Conference (PVSC) 35th IEEE* (2010) Honolulu, HI, p. 001259.
 - ⁶ O. Khaselev, A. Bansal, J.A. Turner, *Int. J. Hydrogen Energ.* **26** (2001) 127.
 - ⁷ A. J. Bard and M. A. Fox, *Acc. Chem. Res.* **28** (1995) 141.
 - ⁸ B. Marsen, S. Dorn, B. Cole, R. E. Rocheleau, E. L. Miller, *Mater. Res. Soc. Symp. Proc.* 974E, Warrendale, PA, 2007, 0974-CC09-05.
 - ⁹ J. Leisch, J. Abushama, and J. A. Turner, *ECS Meeting Abstracts* **502** (2006) 821-821.
 - ¹⁰ B. Marsen, B. Cole, E. L. Miller, *Sol. Energy Mater. Sol. Cells*, doi:10.1016/j.solmat.2008.03.009 (2008).
 - ¹¹ M. Turcu and U. Rau, *J. Phys. Chem. Solids* **64** (2003) 1591.
 - ¹² S. B. Zhang, S.-H. Wei, A. Zunger, *J. Appl. Phys.* **83** (1998) 3192.
 - ¹³ D. Schmid, M. Ruckh, F. Grunwald, H. W. Schock, *J. Appl. Phys.* **73** (1993) 2902.
 - ¹⁴ M. Bär, S. Nishiwaki, L. Weinhardt, S. Pookpanratana, O. Fuchs, M. Blum, W. Yang, J.D. Denlinger, W.N. Shafarman, C. Heske, *Appl. Phys. Lett.* **93** (2008) 244103.
 - ¹⁵ S.-H. Wei and A. Zunger, *J. of Appl. Phys.* **78** (1995) 3846-3856.
 - ¹⁶ L. Weinhardt, Dissertation Thesis, University Wurzburg, **2005**.
 - ¹⁷ J. Kaneshiro, A. Deangelis, N. Gaillard, Y. Chang, J. Kowalczyk, E.L. Miller, *Photovoltaic Specialists Conference (PVSC) 35th IEEE* (2010) Honolulu, HI, p.002448.
 - ¹⁸ H. Wang, *Int. J. Photoenergy* (2011) 801292.
 - ¹⁹ T. K. Todorov, K. B. Reuter, D. B. Mitzi *Adv. Mater.* **22** (2010) E156
 - ²⁰ D. Yokoyama, T. Minegishi, K. Jimbo, T. Hisatomi, G. Ma, M. Katayama, J. Kubota, H. Katagiri, K. Domen, *Appl. Phys. Express* **3** (2010) 101202.
 - ²¹ G. Ma, T. Minegishi, D. Yokoyama, J. Kubota, K. Domen, *Chem. Phys. Lett.* **501** (2011) 619-622.
 - ²² M. Miyauchi, T. Hanayama, D. Atarashi, E. Sakai, *J. Phys. Chem. C* **116** (2012) 23945-23950.
 - ²³ T. Kameyama, T. Osaki, K. Okazaki, T. Sibayama, A. Kudo, S. Kuwabata, T. Torimoto J. *Mater. Chem.* **20** (2010) 5319-5324.
 - ²⁴ S. C. Riha, S. J. Fredrick, J. B. Sambur, Y. Liu, A. L. Prieto, B. A. Parkinson *ACS Appl. Mater. Interfaces* **3** (2011) 58-66

PEC White Papers: WO₃ for PEC Hydrogen Production

The viability for using tungsten oxide based compounds as a photoelectrode for the solar production of hydrogen.

Nicolas Gaillard^a, Yat Li^b, Heli Wang^c

a. Hawaii Natural Energy Institute

b. University of California, Santa Cruz

c. National Renewable Energy Laboratory

Synopsis:

Tungsten trioxide (WO₃) is an *n*-type semiconductor that has been chosen as a model material to validate the concept of photoelectrochemical (PEC) water splitting. WO₃ has been an ideal photoanode material in the study of PEC water-splitting systems because it inherently has good photon absorption generating decent amount of photocurrent, good electron transport properties, and stability against (photo)corrosion. In practice, WO₃ photoanodes have been implemented in prototype multijunction PEC systems including hybrid photoelectrodeⁱ and dual photoelectrode cell approachⁱⁱ. As the basis for a thin-film photoanode in an efficient water-splitting device, pure WO₃ falls short on two principal fronts. The first barrier is a bandgap (between 2.5-2.8 eV) that is too high to absorb an adequate portion of the solar spectrum. As experimentally validated, the high bandgap limits achievable photocurrents, resulting in devices with solar to hydrogen (STH) conversion efficiencies which do not exceed 3 percentⁱⁱⁱ. In perspective, optimized material systems will be needed to meet the DOE's 2020 benchmark of 20% STH conversion efficiency. A second barrier for pure WO₃ is the non-optimal band-edge alignment of the conduction band. PEC experiments on WO₃ films in acidic aqueous media have indicated a conduction band minimum that is lower than the hydrogen evolution reaction reduction potential. In the photoanode configuration, this non-favorable band-edge alignment results in the need for a supplemental voltage bias, complicating the design of practical water-splitting devices. As we continue forward in the R&D of tungsten-based compounds, the primary thrust of our research plan is focus on the bandgap and band-edge alignment issues. Based on comprehensive theoretical and experimental feedback efforts, new multi-component tungsten-based compounds are being developed with raised valence band maximum and conduction band minimum, ideally resulting in a sufficiently low bandgap for high photocurrents and favorable band-edge alignment to minimize or eliminate voltage bias requirements. Materials processing and stability issues for promising new compounds are also be addressed.

Technology Barriers:

Although pure WO₃ is not sufficient to meet DOE's long-term PEC hydrogen generation via water-splitting performance targets, tungsten-based compounds show great promise with respect to the three major materials-related barriers listed in the US DOE EERE Hydrogen program plan. This section highlights the challenges and strengths of

PEC White Papers: WO₃ for PEC Hydrogen Production

tungsten-based compounds in this context, and outlines research solution pathways specific to this material class.

Addressing the Challenges^{iv}:

- Y. Materials Efficiency. Different approaches are currently being evaluated to address WO₃ bandgap reduction, band-edge alignment with water redox potential and optimized surface activity. Incorporation of ions into WO₃ bulk film can be performed to enhance absorption properties (i.e. bandgap reduction), as predicted by density functional theory calculation.
- Z. Materials Durability. Long-term stability in acidic media needs to be evaluated on tungsten oxide-based materials.
- AB. Bulk Materials Synthesis. Several techniques including sol-gel, CVD and reactive sputtering are ideally suited to this material. Other methods such as Atomic Layer Deposition (ALD) should be evaluated.
- AC. Device Configuration Designs. For initial studies, the multijunction device structure can be validated via mechanical stacks (already validated with WO₃). With identification of an ideal top PEC material, the engineering of the complete multi-junction device will be concluded. Work on fully integrated (monolithic) devices will require close collaboration with our industrial partner (MVSystem).

Research Status:

a. Improving WO₃ optical absorption

The reduction of optical bandgap remains the most important task for this material class. Based on theoretical calculation^v, a series of foreign elements have been incorporated into tungsten trioxide bulk, including sulfur and nitrogen. In both cases, no clear evidence of bandgap reduction was observed, although absorption characteristics were impacted by these treatments. A closer look at UV-visible spectra revealed possible free carrier absorption for WO₃:N and WO₃:S systems which could originate from defect points in the newly formed systems. It is worth mentioning that structural characterization (X-ray analysis) pointed out a dramatic phase modification after foreign element incorporation, from monoclinic/orthorhombic (known structures for WO₃) to cubic-like system. The later could emerge only if a high concentration of defects (oxygen vacancies) is present in the material. Subsequent PEC characterization pointed out poor performances when compared to pure WO₃ material; mostly related to weak carrier transport due to grain structure degradation^{vi}. It is worth mentioning that in the nitrogen case, XPS analyses performed at UNLV at newly formed thin film surface has not revealed so far the presence of any nitrogen species, indicating weak bonds between involved species. Tungsten oxide alloying with foreign elements has been also reported by Pr. Augustynski (Warsaw University) and Dr. Braun (EMPA). Their study shown that Si, Ru, Li, and Mo had a pronounced impact on the morphology of the resulting WO₃

PEC White Papers: WO₃ for PEC Hydrogen Production

alloys (synthesized via sol-gel method), improving electrochromic characteristics^{vii}. However, water-splitting experiments indicated a net decrease of saturated photocurrent density under AM1.5G illumination.

b. Near-surface engendering with bilayer approach

Encouraging results have been obtained when Mo is incorporated at the WO₃ surface only (bilayer structure). A 15% enhancement of the generated photocurrent at 1.6V vs SCE as well as a 200 mV onset potential reduction (tested under simulated AM1.5G illumination in 0.33M H₃PO₄ electrolyte) were observed^{viii}. It is believed that improved bilayer performances may come from a beneficial effect of the WO₃ bottom layer on Mo:WO₃ grain growth. In fact, bilayer structure shows highly crystalline grains when compared to those of bulk Mo:WO₃ materials (Mo incorporation in the whole film). High-resolution TEM characterizations performed at NREL indeed validated this point. Further electron spectroscopy analyses (UPS and IPES) performed at UNLV pointed out that Mo incorporation into WO₃ leads to a conduction band-edge position increase of 210 meV^{ix} when compared to pure tungsten trioxide^x. In a bilayer configuration, this difference in Fermi level position leads to the formation of built in potential which direction and strength promotes photogenerated holes diffusion toward the PEC material/electrolyte interface.

c. Surface catalysis of WO₃

First evaluation of RuO₂ particle deposition on WO₃ films has been evaluated by UCSB for catalytic purposes. RuO₂ particles have been either deposited using an electrochemical process on HNEI reactively sputtered WO₃ or deposited using spray pyrolysis on UCSB electrodeposited WO₃. No major improvement in either saturated photocurrent or the onset potential has been observed after RuO₂ surface treatment. In a second phase, HNEI developed a RuO₂ nanoparticle sputtering process using a pure Ru target in oxidizing environment. By adjusting the deposition duration (basically less than 30 seconds), RuO₂ nanoparticles (5-10 nm mean size) were successfully deposited on tungsten trioxide thin films. Subsequent PEC characterization indicated a 20% increase in photocurrent density at a low potential while the onset potential and the saturated photocurrent remained unchanged. This is a clear indication that surface catalysis was effectively addressed with RuO₂ treatmentⁱⁱⁱ. In addition, full sheet RuO₂ films have been fabricated at HNEI using identical process. Tests in a two electrode configuration using p-type material (CGSe or a-SiC) as working electrode and an optimal RuO₂ film as counter electrode have already shown improved results, i.e. a 500 mV onset potential reduction when compared to Pt counter electrodeⁱⁱⁱ.

d. Assessment of WO₃ stability in acidic media

Durability tests were performed by HNEI on reactively sputtered WO₃ thin films in 0.33M H₃PO₄ electrolyte under a constant potential of 1.6V vs. SCE. Several light sources were evaluated as an alternative to costly (and short lifespan) Xe-arc bulbs usually used to mimic AM1.5G illumination. Tungsten bulbs were ruled out as they do

PEC White Papers: WO₃ for PEC Hydrogen Production

not emit enough UV. Decision was made to use UV-white LED light bulbs instead. Under these conditions, a fairly steady photocurrent density of 1.5 mA/cm² was recorded on five WO₃ samples over 1,200 hours. As this current density represents only half of that usually measured under simulated AM1.5_G illumination, the time of operation reported was therefore divided by a factor of two, i.e. 600 hours, to be consistent with the amount of coulombs that would pass through a WO₃ hybrid system generating hydrogen at a STH of 3.2% (benchmark).

e. Integration of WO₃ into a monolithic device

Since hydrogen production using a standalone device is our main goal, efforts have been made to combine both a-Si tandem solar cells and tungsten trioxide PEC electrode in one monolithically integrated device. The main barrier in this task lies in the process temperature incompatibility between the engine (a-Si) and the PEC material (WO₃). HNEI demonstrated via temperature cycling that WO₃ couldn't be integrated in traditional hybrid structure where the PEC material is deposited on top of the PV system, as a-Si solar cells degrades rapidly when exposed to 300°C for 3 hours (WO₃ sputtering deposition parameters). The solution resides in a bifacial integration, where the tungsten oxide film is deposited first on the front side of the transparent conductive oxide (TCO) substrate (performed at HNEI) followed by the deposition of the solar cell on the backside (performed at MVS). First monolithic devices were successfully fabricated in 2011 and tested under out-door conditions. Although, the overall STH efficiency (1.5%) was lower than that obtained with mechanical stacks (3%), this demonstration proved that the concept was feasible. It is worth mentioning that the limiting factor in this integration scheme is no longer the a-Si material but the TCO substrate which can withstand temperatures up to 550°C. This makes the bifacial approach compatible with numerous PEC materials, including I-III-VI₂ (e.g. CuGaSe₂).

Future of tungsten trioxide in PEC research:

With an optical bandgap of 2.6 eV, tungsten trioxide theoretical STH cannot exceed 6% and will not reach the target fixed by DOE. Efforts have been done in the past to decrease WO₃ bandgap using foreign elements incorporation but effective reduction has not been reported yet. Although not optimum as core solar absorber, it still attracts lots of interests, mainly due to its good transport properties and resistance to corrosion. Tungsten trioxide has been the workhorse of PEC since the early ages of photochemistry. Lots of new concepts have been developed on this model system before being implemented to other PEC materials. Examples include the development of monolithic bifacial hybrid device recently reported by HNEI and MVS as well as the introduction of RuO₂ material as a counter electrode in photocathode-based systems. Several papers have been also published on the use of WO₃ in dye sensitized solar cells^{xi}, PEC dual photo-electrode systemsⁱⁱ and for methanol oxidation^{xii}. In the context of pure water splitting, tungsten trioxide could serve as an excellent capping layer sitting on top of a more efficient (yet non-resistant to corrosion) photoanode. The later is supported by the fact that WO₃ is an excellent oxygen evolution catalyst.

PEC White Papers: WO₃ for PEC Hydrogen Production**References**

-
- ⁱ E. Miller, R. Rocheleau, X. Deng, “Design Considerations for a Hybrid Amorphous Silicon / Photoelectrochemical Multijunction Cell for Hydrogen Production”, *Int. J. Hydrogen Energy*, 2003, 28(6), 615-623.
- ⁱⁱ Wang, H.; Deutsch, T.; Turner, J. A. (2008). "Direct Water Splitting Under Visible Light with a Nanostructured Hematite and WO₃ Photoanodes and a GaInP₂ Photocathode". *J. Electrochem. Soc.*, 155, F91 (2008).
- ⁱⁱⁱ N. Gaillard, Y. Chang, J. Kaneshiro, A. Deangelis and E. L. Miller, “Status of Research on Tungsten Oxide-based Photoelectrochemical Devices at the University of Hawai’i”, *Proc. SPIE*, Vol. 7770, 77700V; doi:10.1117/12.860970 (2010).
- ^{iv} Fuel Cell Technologies Program Multi-Year Research, Development and Demonstration Plan, updated September 2011, US DOE, Office of Energy Efficiency and Renewable Energy, Page 3.1 – 27, <http://www1.eere.energy.gov/hydrogenandfuelcells/mypp/index.html>
- ^v M.N. Huda, Y. Yan, C-Y. Moon, S-H. Wei, and M.M. Al-Jassim: Density-functional theory study of the effects of atomic impurity on the band edges of monoclinic WO₃. *Phys. Rev. B* 77, 195102 (2008).
- ^{vi} B. Cole, B. Marsen, E.L. Miller, Y. Yan, B. To, K. Jones, and M.M. Al-Jassim: Evaluation of nitrogen doping of tungsten oxide for photoelectrochemical water splitting. *J. Phys. Chem. C* 112, 5213 (2008).
- ^{vii} R. Solarska, B.D. Alexander, A. Braun, R. Jurczakowski, G. Fortunato, M. Stiefel, T. Graule, J. Augustynski, “Tailoring the morphology of WO₃ films with substitutional cation doping: Effect on the photoelectrochemical properties”, Volume 55, Issue 26, 1 November 2010, Pages 7780–7787
- ^{viii} Gaillard, N.; Cole, B.; Marsen, B.; Kaneshiro, J.; Miller, E. L.; Weinhardt, L.; Bar, M.; Heske, C. “Improved current collection in WO₃:Mo/WO₃ bilayer photoelectrodes”, *J. Mater. Res.* 2010, 25, 1–7.
- ^{ix} M. Bär, L. Weinhardt, B. Marsen, B. Cole, N. Gaillard, E. Miller, and C. Heske, “Mo incorporation in WO₃ thin film photoanodes: Tailoring the electronic structure for photoelectrochemical hydrogen production”, *Appl. Phys. Lett.* 96, 032107 (2010).
- ^x L. Weinhardt, M. Blum, M. Bar, C. Heske, B. Cole, B. Marsen, and E.L. Miller: Electronic surface level positions of WO₃ thin films for photoelectrochemical hydrogen production. *J. Phys. Chem. C* 112, 3078 (2008).
- ^{xi} Satyen K. Deb, “Opportunities and challenges in science and technology of WO₃ for electrochromic and related applications”, *Solar Energy Materials & Solar Cells* 92 (2008) 245–258.
- ^{xii} D. V. Esposito, J. G. Chen, R. W. Birkmire, Y. Chang, N. Gaillard, “Hydrogen production from photo-driven electrolysis of biomass-derived oxygenates: A case study on methanol using Pt-modified WO₃ thin film electrodes”, *Int. J. Hydrogen Energ.* 36, 9632 (2011).

PEC White Papers: MoS₂ for PEC hydrogen production

Molybdenum Disulfide for Photoelectrochemical Water Splitting

Z. Chen, J.D. Benck, and T.F. Jaramillo, Department of Chemical Engineering, Stanford University

Introduction

Photoelectrochemical (PEC) water splitting provides a promising method for producing hydrogen from water using the energy from sunlight. However, there currently exists no material system that can perform this process efficiently and economically.

Molybdenum disulfide (MoS₂) is a promising candidate photocathode material for PEC water splitting. MoS₂ is a dichalcogenide semiconductor with a bulk band gap of ~1.2 eV that occurs naturally in n-type and p-type forms.¹ The crystal structure of MoS₂ consists of parallel S-Mo-S planes bound loosely through van der Waals forces.¹ This material is advantageous because it is composed of abundant elements, can be synthesized using inexpensive processes, and is stable to corrosion at reductive potentials.^{1,2}

Significant foundational work assessing the viability of MoS₂ as a photoelectrode was performed decades ago by leading researchers in the field of photoelectrochemistry. Seminal studies by Tributsch and Bennett in 1977 showcased the photoactivity of n-MoS₂ as well as p-MoS₂.³ Studies by Kautek and Gerischer,⁴ Gobrecht et al.,⁵ as well as Schneemeyer and Wrighton⁶ further characterized various properties of MoS₂, including its flat-band potential and band structure.

Several groups have also investigated the photocorrosion of MoS₂. Fujishima performed studies of MoS₂ mounted in a rotating ring disk electrode geometry and showed that photogenerated holes in n-MoS₂ kinetically favor the corrosion of the surface into SO₄²⁻ and Mo⁶⁺ species rather than water oxidation, while photogenerated electrons drive H⁺ reduction into H₂.⁷ However, the addition of a I/I₂ redox couple could stabilize the surface and also shift the position of the flat-band potential. Similarly, Kubiak et al. showed that the addition of Cl⁻ and Br⁻ in solution at high concentrations could limit corrosion.⁸

Further work focused on characterizing the performance of micro- or nanostructured MoS₂ photoelectrodes. Kiesewetter et al. attempted to incorporate microcrystals of MoS₂ as the absorber in a dye sensitized solar cell with a TiO₂ support and I⁻/I₃⁻ redox couple.⁹ However, this approach yielded relatively low activity compared to bulk MoS₂. Since nanostructured materials often have a higher density of surface defect sites, this result was consistent with previous studies by Kline et al., who demonstrated that highly structured MoS₂ with surface steps produced lower photoactivity.¹⁰ The cause was found to be due to a high rate of recombination at these surface steps, as elucidated by Furtak and Parkinson in studies of other layered chalcogenide materials such as WSe₂.^{11,12}

Technical Challenges

To successfully incorporate MoS₂ into a functional and economical water splitting photocathode, several materials requirements established for a single-band gap PEC device must be met.¹³⁻¹⁶ Designing nanostructures to tune the properties of MoS₂ to meet these requirements presents the following technical challenges:

PEC White Papers: MoS₂ for PEC hydrogen production

1. Catalysis

MoS₂ must efficiently catalyze the hydrogen evolution reaction to minimize efficiency losses due to kinetic overpotential. The bulk form of MoS₂ consists primarily of extended flat basal planes of S-Mo-S layers, which serve as poor catalysts for hydrogen evolution¹ because proton adsorption is energetically unfavorable. In contrast, the edge sites of the basal planes are highly active for hydrogen evolution.^{17,18} Therefore, the design of nanostructures that maximizes the exposure of active edge sites is an important technical challenge for improving the performance of MoS₂.

2. Band Gap

The band gap of MoS₂ must be sufficiently large to overcome the thermodynamic and kinetic energy requirements for splitting water. The band gap of bulk MoS₂ is approximately 1.2 eV,^{19,20} which is too small to split water without an additional potential bias. An internal (rather than external) bias could potentially be provided by utilizing a vertically stacked tandem device structure with a separate absorber. Nanostructuring is another approach that can be used to increase the band gap of MoS₂ through quantum confinement. Further work is required to apply this strategy to appropriate MoS₂ morphologies and to incorporate quantum confined MoS₂ structures into a PEC water splitting device.^{20,21} In the absence of a sufficient band gap to drive unassisted water splitting, MoS₂ may still be incorporated into a multi-absorber configuration with a matching photoanode. In either case (single absorber or multi-absorber), voltage losses from the band gap due to factors such as insufficient light trapping and non-radiative recombination need to be minimized. The former challenge arises from the highly reflective nature of a flat MoS₂ surface, whereas the latter recombination arises from the indirect band gap nature of bulk MoS₂.

3. Charge Carrier Transport and Conversion Efficiency

Excited charge carriers must reach the semiconductor-electrolyte interface prior to recombination. Due to its layered structure, mobility in MoS₂ is highly anisotropic. While charge transport along S-Mo-S layers is rapid ($\sim 200 \text{ cm}^2 \text{ V}^{-1} \text{ s}^{-1}$), mobility perpendicular to the S-Mo-S layers is more than 2000 times lower.¹ Therefore, slow transport of excited charge carriers can limit device performance in bulk MoS₂. Nanostructured MoS₂ can overcome this limitation by reducing the distance charge carriers must travel before reaching the semiconductor surface, minimizing resistive as well as bulk recombination losses. However, nanostructuring may also lead to increased surface recombination, which can decrease carrier collection efficiency.²² Strategies such as surface passivation may be required to avoid this potential pitfall while maintaining the benefits of decreased carrier collection path lengths in nanostructured MoS₂ photoelectrodes.

4. Device Configuration

While nanostructuring MoS₂ provides many benefits for catalysis, band structure, and charge transport, it also imposes some additional challenges for integrating this material into a functional PEC water splitting electrode. Due to their small size, some MoS₂ nanostructures have absorption path lengths that are too short to capture a large fraction of incident sunlight, as is necessary to achieve high energy conversion efficiency. Therefore, the development of device configurations that maximize light absorption while maintaining the benefits of nanostructuring is crucial. In particular, it may be necessary to combine MoS₂ nanostructures with high aspect ratio support architectures, incorporate light trapping structures, or utilize plasmonic effects to enhance light absorption.²³⁻²⁵ This may also necessitate the development of novel synthesis techniques for MoS₂. In the past, the synthesis of MoS₂ typically required treatment in H₂S gas at high temperatures ($>400^\circ\text{C}$).^{18,26-28} The presence of H₂S sulfidizing agent at these temperatures is extremely corrosive, which prevents the integration of MoS₂ into many potential support structures.

PEC White Papers: MoS₂ for PEC hydrogen production

5. Stability

MoS₂ is not stable in alkaline (base) electrolytes. However, it is quite stable in acidic electrolytes, and is commonly characterized in concentrated sulfuric acid.^{29,30} Furthermore, while MoS₂ corrodes at oxidative potentials,^{1,31} it is highly stable at the potentials required for hydrogen evolution, i.e. more negative than 0 V vs RHE, and does not anodically corrode until potentials more positive than 0.5 V vs. RHE.^{29,30} For some potential device configurations, it may be necessary to develop strategies for stabilizing or protecting the MoS₂ surface to prevent corrosion at oxidative potentials.

Research Status

Although the charge transport properties of MoS₂ are not ideal in bulk form due to the anisotropic conductivity of its layered structure,¹ core-shell MoO₃-MoS₂ nanowires demonstrate that thin conformal MoS₂ films of only a few nanometers in thickness exhibit negligible ohmic resistance due to the small length scale for carrier transport. Additionally, the conformal ultrathin MoS₂ shell completely protects the high aspect ratio MoO₃ core architecture, which by itself is unstable and rapidly corrodes in strong acids and at cathodic potentials. This structure remained stable in strong acid for more than 10,000 simulated diurnal cycles.²⁹ The stability exhibited by core-shell nanostructures opens the opportunity to study thin conformal layers of MoS₂ as a simultaneous stabilizing agent and highly efficient electrocatalyst for photocathodes.³²

Significant advances have been made in developing novel synthetic procedures for MoS₂ that broaden the parameter space for its integration into device morphologies. Recent MoS₂ nanostructures are synthesized at atmospheric pressure at considerably lower (200°C) temperatures,²⁹ enabling the use of oxide substrates such as fluorine-doped tin oxide (FTO). Highly active electrocatalysts of amorphous MoS_x have also been synthesized at room temperature under atmospheric pressure or low vacuum without employing any H₂S, which may enable the facile deposition of this material onto many types of substrates.³³⁻³⁵

Approaches

While some properties of bulk MoS₂, including its band gap and catalytic activity, are insufficient to enable unassisted water splitting, nanostructuring provides a means to enhance this material's favorable properties while simultaneously mitigating its deficiencies. Nanostructured MoS₂ has the potential to satisfy all the requirements necessary to create a practical PEC photocathode.

The recent development of novel MoS₂ nanostructures with unique electrocatalytic, electronic, and optical properties has highlighted the potential of MoS₂ for integration into PEC water splitting devices. Various MoS₂ nanostructures have demonstrated excellent activity for hydrogen evolution electrocatalysis. These structures include core-shell nanowires of MoO₃-MoS₂,²⁹ mesoporous MoS₂ thin films, and nanoparticulate MoS₂ thin films. All of these nanostructures increase the density of active edge sites in contact with the electrolyte, and therefore act as highly efficient catalysts for hydrogen evolution, surpassing the activity of MoS₂ nanoclusters studied previously¹⁸ and achieving solar-to-hydrogen-relevant current densities of 10 mA/cm² at ~200 mV overpotential.

Nanostructuring MoS₂ also serves as a route to engineer novel semiconducting properties. MoS₂ nanoparticles in the regime of < 10 nm exhibit blueshifts in the onset of optical absorption corresponding to a band gap enlargement characteristic of quantum confinement.^{20, 36, 37} In 2 – 5 nm diameter nanoparticles, the band gap of MoS₂ can be increased to more than 2 eV,^{2, 20, 37} which may be sufficient to split water without an external bias. Recently, single monolayers of exfoliated MoS₂ crystals have exhibited direct band gap photoluminescence which is not observed in the bulk form.³⁸⁻⁴⁰ These single monolayer crystallites further exhibit high charge mobilities of >200 cm² V⁻¹ s⁻¹ along the (0001) plane,^{41,}

PEC White Papers: MoS₂ for PEC hydrogen production

⁴² renewing interest in MoS₂ as a material for electronic applications.^{43,44} These studies show that nanostructuring provides an effective means for tuning the band structure of MoS₂.

Although some of the technical challenges associated with the development of nanostructured MoS₂ photocathodes have been thoroughly addressed in recent studies, more progress is required to make this material viable for PEC water splitting. In particular, the limitations of charge transport, conversion efficiency, and device configuration remain major challenges.

The precise mechanisms that lead to charge carrier recombination in nanostructured MoS₂ are not well understood. Crystallographic defects such as grain boundaries, screw dislocations, atomic vacancies, interstitial atoms, or under-coordinated surface sites could create mid-band gap energy states that act as recombination centers. A recent study suggested that the edge sites responsible for the high catalytic activity of MoS₂ may also serve as recombination centers.⁴⁵ Further work using techniques such as time-resolved photoluminescence^{46,47} will be necessary to elucidate the nature of these various factors and enable improved material design.

References

1. Tributsch, H.; Bennett, J. C. *J. Electroanal. Chem.* **1977**, 81, (1), 97-111.
2. Wilcoxon, J. P.; Samara, G. A. *Phys. Rev. B* **1995**, 51, (11), 7299-7302.
3. Tributsch, H.; Bennett, J. C. *J. Electroanal. Chem.* **1977**, 81, (1), 97-111.
4. Kautek, W.; Gerischer, H. *Ber. Bunsen-Ges. Phys. Chem. Chem. Phys.* **1980**, 84, (7), 645-653.
5. Gobrecht, J.; Tributsch, H.; Gerischer, H. *J. Electrochem. Soc.* **1978**, 125, (12), 2085-2086.
6. Schneemeyer, L. F.; Wrighton, M. S. *J. Am. Chem. Soc.* **1979**, 101, (22), 6496-6500.
7. Fujishima, A.; Noguchi, Y.; Honda, K.; Loo, B. H. *Bull. Chem. Soc. Jpn.* **1982**, 55, (1), 17-22.
8. Kubiak, C. P.; Schneemeyer, L. F.; Wrighton, M. S. *J. Am. Chem. Soc.* **1980**, 102, (22), 6898-6900.
9. Kiesewetter, T.; Tamm, Y.; Turrion, M.; Tributsch, H. *Sol. Energy Mater. Sol. Cells* **1999**, 59, (4), 309-323.
10. Kline, G.; Kam, K. K.; Ziegler, R.; Parkinson, B. A. *Solar Energy Materials* **1982**, 6, (3), 337-350.
11. Parkinson, B. A.; Furtak, T. E.; Canfield, D.; Kam, K. K.; Kline, G. *Faraday Discussions* **1980**, 70, 233-245.
12. Furtak, T. E.; Canfield, D. C.; Parkinson, B. A. *J. Appl. Phys.* **1980**, 51, (11), 6018-6021.
13. Bak, T.; Nowotny, J.; Rekas, M.; Sorrell, C. C. *Int. J. Hydrog. Energy* **2002**, 27, (10), 991-1022.
14. Aroutiounian, V. M.; Arakelyan, V. M.; Shahnazaryan, G. E. *Sol. Energy* **2005**, 78, (5), 581-592.
15. Nowotny, J.; Sorrell, C. C.; Sheppard, L. R.; Bak, T. *Int. J. Hydrog. Energy* **2005**, 30, (5), 521-544.
16. Walter, M. G.; Warren, E. L.; McKone, J. R.; Boettcher, S. W.; Mi, Q. X.; Santori, E. A.; Lewis, N. S. *Chem. Rev.* **2010**, 110, (11), 6446-6473.
17. Hinnemann, B.; Moses, P. G.; Bonde, J.; Jorgensen, K. P.; Nielsen, J. H.; Horch, S.; Chorkendorff, I.; Norskov, J. K. *J. Am. Chem. Soc.* **2005**, 127, (15), 5308-5309.
18. Jaramillo, T. F.; Jorgensen, K. P.; Bonde, J.; Nielsen, J. H.; Horch, S.; Chorkendorff, I. *Science* **2007**, 317, (5834), 100-102.
19. Coehoorn, R.; Haas, C.; Dijkstra, J.; Flipse, C. J. F.; Degroot, R. A.; Wold, A. *Physical Review B* **1987**, 35, (12), 6195-6202.
20. Wilcoxon, J. P.; Newcomer, P. P.; Samara, G. A. *J. Appl. Phys.* **1997**, 81, (12), 7934-7944.
21. Chen, Z.; Kibsgaard, J.; Jaramillo, T. F. In *Nanostructuring MoS₂ for photoelectrochemical water splitting*, 2010; Hicham, I.; Heli, W., Eds. SPIE: 2010; p 77700K.
22. Osterloh, F. E. *Chem. Soc. Rev.* **2013**.
23. Zhu, J.; Hsu, C. M.; Yu, Z. F.; Fan, S. H.; Cui, Y. *Nano Lett.* **2010**, 10, (6), 1979-1984.

PEC White Papers: MoS₂ for PEC hydrogen production

24. Zhu, J.; Yu, Z. F.; Burkhard, G. F.; Hsu, C. M.; Connor, S. T.; Xu, Y. Q.; Wang, Q.; McGehee, M.; Fan, S. H.; Cui, Y. *Nano Lett.* **2009**, 9, (1), 279-282.
25. Thomann, I.; Pinaud, B. A.; Chen, Z.; Clemens, B. M.; Jaramillo, T. F.; Brongersma, M. L. *Nano Letters* **2011**, 11, (8), 3440-3446.
26. Margulis, L.; Salitra, G.; Tenne, R.; Talianker, M. *Nature* **1993**, 365, (6442), 113-114.
27. Zak, A.; Feldman, Y.; Alperovich, V.; Rosentsveig, R.; Tenne, R. *J. Am. Chem. Soc.* **2000**, 122, (45), 11108-11116.
28. Bonde, J.; Moses, P. G.; Jaramillo, T. F.; Norskov, J. K.; Chorkendorff, I. *Faraday Discuss.* **2008**, 140, 219-231.
29. Chen, Z.; Cummins, D.; Reinecke, B. N.; Clark, E.; Sunkara, M. K.; Jaramillo, T. F. *Nano Lett.* **2011**, 11, (10), 4168-4175.
30. Li, Y. G.; Wang, H. L.; Xie, L. M.; Liang, Y. Y.; Hong, G. S.; Dai, H. J. *J. Am. Chem. Soc.* **2011**, 133, (19), 7296-7299.
31. Kautek, W.; Gerischer, H. *Surf. Sci.* **1982**, 119, (1), 46-60.
32. Zong, X.; Yan, H.; Wu, G.; Ma, G.; Wen, F.; Wang, L.; Li, C. *J. Am. Chem. Soc.* **2008**, 130, (23), 7176-7177.
33. Merki, D.; Fierro, S.; Vrabel, H.; Hu, X. L. *Chem. Sci.* **2011**, 2, (7), 1262-1267.
34. Merki, D.; Hu, X. *Energy & Environmental Science* **2011**, 4, (10), 3878-3888.
35. Benck, J. D.; Chen, Z.; Kuritzky, L. Y.; Forman, A. J.; Jaramillo, T. F. *ACS Catalysis* **2012**, 1916-1923.
36. Wilcoxon, J. P.; Samara, G. A. *Phys. Rev. B, Condens. Matter* **1995**, 51, (11), 7299-7302.
37. Thurston, T. R.; Wilcoxon, J. P. *J. Phys. Chem. B* **1999**, 103, (1), 11-17.
38. Mak, K. F.; Lee, C.; Hone, J.; Shan, J.; Heinz, T. F. *Phys. Rev. Lett.* **2010**, 105, (13).
39. Splendiani, A.; Sun, L.; Zhang, Y.; Li, T.; Kim, J.; Chim, C.-Y.; Galli, G.; Wang, F. *Nano Lett.* **2010**, 10, (4), 1271-1275.
40. Eda, G.; Yamaguchi, H.; Voiry, D.; Fujita, T.; Chen, M.; Chhowalla, M. *Nano Lett.* **2011**, 11, (12), 5111-5116.
41. Fivaz, R.; Mooser, E. *Physical Review* **1967**, 163, (3), 743-755.
42. Mansfield, R.; Salam, S. A. *Proceedings of the Physical Society of London Section B* **1953**, 66, (401), 377-385.
43. Radisavljevic, B.; Radenovic, A.; Brivio, J.; Giacometti, V.; Kis, A. *Nature Nanotech.* **2011**, 6, (3), 147-150.
44. Yoon, Y.; Ganapathi, K.; Salahuddin, S. *Nano Lett.* **2011**, 11, (9), 3768-3773.
45. Chen, Z.; Forman, A. J.; Jaramillo, T. F. *The Journal of Physical Chemistry C* **2013**, 117, (19), 9713-9722.
46. Doolen, R.; Laitinen, R.; Parsapour, F.; Kelley, D. F. *J. Phys. Chem. B* **1998**, 102, (20), 3906-3911.
47. Parsapour, F.; Kelley, D. F.; Craft, S.; Wilcoxon, J. P. *Journal of Chemical Physics* **1996**, 104, (13), 4978-4987.

PEC White Papers: Engineered Oxide Minerals

Engineered ternary and quaternary oxide minerals with optimal absorption characteristics for solar-assisted low-cost hydrogen production.

Nicolas Gaillard^a, Muhammad N. Huda^b

- a. Hawaii Natural Energy Institute
- b. The University of Texas in Arlington

Synopsis:

Four decades after the demonstration of photoelectrochemical (PEC) water splitting by Fujishima and Honda with TiO_2 ⁱ, intensive research is still ongoing to identify a suitable semiconductor to be integrated in an efficient, cost effective, and reliable PEC system. Among all candidates, binary transition metal oxides are still drawing lots of attention as most of them offer good resistance to corrosion and are inexpensive to produce. However, no system having both *appropriate optical absorption* and *good transport properties* have been discovered yet. In the case of wide bandgap materials (i.e. TiO_2 and WO_3), numerous attempts have been made to narrow their bandgaps, mainly via incorporation of foreign element such as nitrogenⁱⁱ. Unfortunately, this method usually leads to an increase in structural defects and poor PEC performancesⁱⁱⁱ. In contrast, hematite ($\alpha\text{-Fe}_2\text{O}_3$) is a material class that already has the right absorption characteristics for solar-powered water splitting. However, hematite falls short on electrical performances, with hole-diffusion length in the order of 20 nm^{iv}, though significant progress in Fe_2O_3 nano-structuring have been made to resolve this issue^{v,vi}. From this point of view, it appears that the one feasible research strategy might be to focus on metal oxides owning appropriate absorption properties and improve, if necessary, their transport and/or catalytic properties.

Nowadays, the optical and electronic properties of all existing binary systems have been studied and are well documented. To the best of our knowledge, only two binary metal oxides can fulfill the requirements in term of band gap for PEC applications: Fe_2O_3 (2.0 eV) and Cu_2O (1.95 eV). In the latter case, recent work by Pr. Grätzel (EPFL) shows that cuprous oxide can generate a photocurrent up to 7 mA/cm² at saturation, making this material the best binary oxide ever synthesized for solar conversion applications^{vii}. The only issue with such system is its thermodynamic stability. Indeed, it is possible that, over time and under operation, cuprous oxide (Cu_2O) turns into cupric oxide (CuO), which bandgap (1.3-1.6 eV) is far from ideal for PEC applications. In the light of these examples, it appears that one need to search beyond binary oxides to find the ideal material for low-cost solar-assisted hydrogen production.

With the increased number of elements in ternary and quaternary compounds comes the difficulty to design a unique system capable of satisfying optical absorption, electronic conductivity and resistance to corrosion. One approach resides in pure combinatorial analysis, where sets of selected elements are automatically blended to form series of compounds. Though rather challenging to perform with vacuum-based processes (e.g. sputtering), recent progress in solution-based (ink) have greatly improved combinatorial-based PEC research and led to the

PEC White Papers: Engineered Oxide Minerals

emergence of interesting new PEC systems[Parkinson]. However, one should bear in mind that the success of such approach should not rely only on opportune material discovery. Similar combinatorial approach has been employed in the past in the field of superconductors to investigate compounds containing multiple cations metal-oxides. While material discoveries in this field used to be quite “serendipitous”^{viii}, modern density functional theory calculation has since permitted to predict trends to design new superconducting material classes.

The ability to design new ternary and quaternary oxide minerals for PEC applications guided by density functional theory predictions defines the objective of this subtask.

Research Status:

a. Copper tungstate

With an electronic band-gap of 2.2 eV and optimum surface energetics for water splitting^{ix,x}, copper tungstate (CuWO_4) is a promising material-class that merits further investigation. Although fairly new in the field of PEC, metal tungstates have been investigated for more than three decades for their scintillation characteristics. A large number of papers have been published on the microstructure and optical characteristics of this material class and metal tungstate-based scintillators are widely used in the field of detection. As an example, calcium tungstate currently equipped the Dark Matter Cryogenic detector at CRESST in Gran Sasso in Italy. Cadmium tungstate is widely used for positron emission tomography in medical diagnosis. Finally, the Electromagnetic Calorimeter detector at the Large Hadron Collider (CERN) is made of approximately 100,000 lead tungstate crystals. In this material class, copper tungstate is the only material with a bandgap (2.2 eV) that is appropriate for PEC applications. However, less than ten papers have been published specifically on the photoelectrochemical properties of CuWO_4 since Benko’s (Brock University) first report in 1982.^{xi} Mott-Schottky analyses reported in 1990 by Arora (Sardar Patel University) on single crystals evidenced that CuWO_4 valence band maximum (VBM) and conduction band minimum (CBM) straddled the oxygen (OER) and hydrogen evolution reaction (HER) potentials, respectively, an ideal situation for solar-assisted water splitting^{xv}. The first thin film CuWO_4 photoelectrode fabrication was reported in 2005 by Pandey (Nagpur University) using spray-deposition method^{xii}. In an attempt to reduce CuWO_4 optical band gap, Chen (NREL) developed a low-temperature co-sputtering process to synthesize amorphous $\text{Cu}_x\text{W}_{(1-x)}\text{O}_4$ thin films^{xiii}. Although copper tungstate absorption characteristics were tunable, amorphous films presented limited photo-response to visible light and were un-stable in aqueous solution. In 2011, Yourey (Michigan) published encouraging results on electrodeposited CuWO_4 ^{xiv} and $\text{CuWO}_4\text{-WO}_3$ ^{xv} composite systems. The authors demonstrated copper tungstate’s stability in a 0.1M Na_2SO_4 solution containing 10% methanol over 12 hours at 0.5 V vs. Ag/AgCl. Finally, Chang (HNEI) reported recently on the effect of thermal treatment on the crystallographic, surface energetics and PEC properties of reactively co-sputtered CuWO_4 ^{ix}. It was observed that thin films fabricated at temperature below 300°C had p-type conductivity and exhibited no significant photoresponse when exposed to Air Mass 1.5_{Global} (AM1.5_G) irradiation. However, a major improvement was observed after a post-annealing at 500°C in argon for 8 hours, exhibiting a photocurrent density of approx. 400 $\mu\text{A}/\text{cm}^2$ at 1.6V vs. SCE. More

PEC White Papers: Engineered Oxide Minerals

importantly, a surface band diagram drawn from electrochemical and optical measurements confirmed Arora's results on the ideal positions of CBM and VBM for solar-assisted water splitting. Electrochemical impedance study also indicated that CuWO_4 transport properties must be improved in order to achieve better performing photoanodes.

b. Down-selection of new oxide minerals via DFT calculation

It has been mentioned earlier that the introduction of impurities for doping would create unwanted defect-states in the band gap, which, in turn, would be detrimental to the crystallinity and the transport properties of the host materials. In addition, the presence of highly localized orbitals at the band edges (such as at the valence band maxima or the conduction band minima of Mott or charge transfer-type insulators), results in high effective mass charge-carriers, and hence high electron-hole recombination rate. On the other hand, a thermodynamically stable alloy structure with desirable materials compositions can provide better crystallinity and, hence improved charge transport properties.

Predicting novel alloys of multi-cation metal oxides satisfying all the electronic criteria of an efficient photocatalyst is a challenge. Nonetheless, recent advances in computers and theoretical methods made it possible to investigate and predict materials at a fundamental level, which were not possible before. In addition, an efficiently combined experiment-theory approach can expedite the prediction and characterization processes further. With our new theoretical approach for materials design by searching mineral data-base, we were able to predict several new tungstate-based multi-cation metal-oxides. For example, from a combined mineral data-based search and DFT calculations, we were able to predict so far unknown crystal structure of AgBiW_2O_8 , and the corresponding electronic properties such as band structure, density of states, optical absorptions, etc. These results were then compared with the experimental findings. We recently have predicted the crystal structure of a new alloy, namely CuBiW_2O_8 , which has a lower band gap and a higher valence band maximum than AgBiW_2O_8 . In contrast to WO_3 , both of these two materials straddle the hydrogen and oxygen reduction potentials. The theoretical XRD plot and other electronic and optical properties will be calculated for the newly predicted material to guide the experimental findings. For example, a predicted XRD plot for CuBiW_2O_8 is shown in the following:

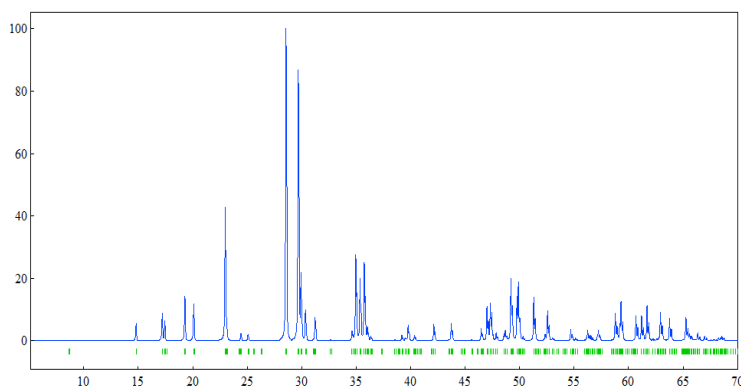


Figure: Calculated XRD plot for CuBiW_2O_8 , a new tungstate based oxide predicted by searching mineral database followed by DFT calculations.

References:

PEC White Papers: Engineered Oxide Minerals

-
- ⁱ Fujishima, A., and Honda, K., *Nature*, 238, 37–38 (1972).
- ⁱⁱ M. Huda, Y. Yan, C.-Y. Moon, S.-H. Wei, M. Al-Jassim, *Physical Review B* 77, 1 (2008).
- ⁱⁱⁱ B. Cole, B. Marsen, E. Miller, Y. Yan, B. To, K. Jones, M. Al-Jassim, *J. Phys. Chem. C* **112**, 5213 (2008).
- ^{iv} Dare-edwards, M. P.; Goodenough, J. B.; Hamnett, A.; Trevellick, P. R. *J. Chem. Soc., Faraday Trans.* 1983, 79, 2027-2041.
- ^v Sivula, K.; Formal, F. L.; Gratzel, M. *ChemSusChem*. 2011, 18, 432-449.
- ^{vi} Vayssieres, L.; Sathe, C.; Butorin, S.; Shuh, D.; Nordgren, J.; Guo, J. *Adv. Mater.* 2005, 17, 2320-2323.
- ^{vii} A. Paracchino; V. Laporte; K. Sivula; M. Grätzel; E. Thimsen. *Nature Materials* 10, 456–461 (2011).
- ^{viii} Basic Research Needs for Supraconductivity, Report of the Basic Energy Sciences, 2006.
- ^{ix} Chang, Y.; Braun, A.; Deangelis, A.; Kaneshiro, J.; Gaillard, N. *J. Phys. Chem. C*, 2011, 115, 25490–25495.
- ^x Arora, S. K.; Mathew T.; Batra, N. M. *J. Phys. D: Appl. Phys.* 1990, 23, 460-464.
- ^{xi} Benko, F. A.; MacLaurin, C. L.; Koffyberg, F. P. *Mat. Res. Bull.* 1982, 17, 133-136.
- ^{xii} Pandey, P. K.; Bhave, N. S.; Kharat, R. B. *Mater. Lett.* 2005, 59, 3149-3155.
- ^{xiii} Chen, L.; Shet, S.; Tang, H.; Ahn, K.; Wang, H.; Yan, Y.; Turner, J.; Jassim, M. A. *J. Appl. Phys.* 2010, 108, 043502 1-5.
- ^{xiv} Yourey J. E.; Bartlett, B. M. *J. Mater. Chem.* 2011, 21, 7651-7660.
- ^{xv} Joseph E. Yourey, Joshua B. Kurtz, and Bart M. Bartlett, *J. Phys. Chem. C*, 2012, 116, 3200–3205.

PEC White Papers: BiVO₄ for PEC hydrogen production

BiVO₄ as a Photoanode for Photoelectrochemical Water Splitting

Kyoung-Shin Choi, Department of Chemistry, University of Wisconsin-Madison, Madison, WI, USA
 Roel van de Krol, Institute for Solar Fuels, Helmholtz-Zentrum Berlin für Materialien und Energie, Berlin, Germany

Introduction

Bismuth vanadate (BiVO₄) has recently emerged as a promising material for use as a photoanode in water-splitting photoelectrochemical cells.^[1,2] It has a bandgap of 2.4 eV with the valence band (VB) edge located at *ca.* 2.4 V vs. RHE (reversible hydrogen electrode), providing sufficient overpotential for holes to photooxidize water while the conduction band (CB) edge is located just short of the thermodynamic level for H₂ production.^[3] Its bandgap is slightly larger than is desired for a photoanode (*ca.* 2.0 eV) but its very negative CB position may compensate for this disadvantage as not many n-type semiconductors that can utilize visible light have a CB edge position that is as negative as that of BiVO₄.^[4,5] In addition, it is composed of only non-precious elements ensuring commercial viability for practical use in large quantities.

In general, oxide semiconductors have wide bandgaps because the VB has mainly the O 2p character and is located at a very positive potential.^[6,7] Therefore, the production of oxide semiconductors that can absorb a significant portion of visible-light requires decreasing their bandgap energies by raising the VB edge. One viable strategy to achieve this is to introduce cations with occupied low binding energy s orbitals such as Bi³⁺ and Sn²⁺.^[6] BiVO₄ is an exemplary case for this approach in that the hybridization of the filled Bi³⁺ 6s² state and O 2p states at the top of the VB effectively shifts the VB edge to the negative direction, reducing the bandgap energy while its CB edge remains at a relatively negative position compared to those of other oxides having comparable bandgaps (e.g. Fe₂O₃, WO₃).

The use of a BiVO₄ photocatalyst for solar oxidation was first reported by Kudo et al. in 1998.^[2] Early work on BiVO₄ mainly focused on suspension-type photocatalysts for water oxidation or photodegradation of organic compounds. Since the CB level does not allow for water reduction, Ag⁺ was typically used as a sacrificial electron acceptor for these studies.

More recent studies on BiVO₄ have focused on the preparation of BiVO₄ as electrode-type materials for use as photoanodes for photoelectrochemical cells. However, the typical efficiencies of unmodified BiVO₄ photoanodes for water oxidation were not impressive as they suffer from excessive electron-hole recombination, poor charge transport properties and poor water oxidation kinetics. Therefore, various strategies such as morphology control, construction of composite structures, doping, and pairing with oxygen evolution catalysts have been developed recently to alleviate one or more of these limitations. Further advancement in the construction of efficient BiVO₄-based photoanode systems is expected once the limitations of BiVO₄ are better understood and new approaches are developed to effectively overcome them.

Technical Challenges

Major technical challenges in constructing highly efficient BiVO₄ photoanodes are summarized below.

1. Light Management

As mentioned earlier, the bandgap of BiVO₄ is slightly larger than is desired for a photoanode. Therefore, theoretical and experimental studies on composition tuning (i.e. formation of solid solutions), which aim to reduce the bandgap (*ca.* 2.0 eV or smaller), are highly desired. To date, no

PEC White Papers: BiVO₄ for PEC hydrogen production

studies on composition tuning have resulted in a decrease in bandgap energy. Ideally, the bandgap reduction should be achieved by elevating the VB edge position without lowering the CB edge position. Engineering the morphology of BiVO₄ electrodes to enhance light absorption is also an important issue.

2. Recombination losses and poor electron transport properties
The separation yield of photogenerated electron and hole pairs in the BiVO₄ system is assessed to be below 30%,^[8,9] making it the main limiting factor for the performance of BiVO₄. Therefore, there is an urgent need for the development of more effective morphologies, compositions (i.e. doping), and cell structures to reduce recombination losses. Undoped BiVO₄ generally shows poor electron transport properties, which appears to be one of the main reasons for the low electron-hole separation yield of BiVO₄. A few doping studies show a significant increase in the photocurrent of BiVO₄.
3. Slow hole transfer kinetics for water oxidation
The surface of BiVO₄ is not particularly catalytic for water oxidation and, therefore, bare BiVO₄ electrodes that are not coupled with oxygen evolution catalysts (OECs) do not show impressive performances for photo-oxidation of water. Coupling of efficient OECs with BiVO₄ without creating undesirable interface states at the BiVO₄/OEC junction is necessary.
4. Chemical and photoelectrochemical stabilities
BiVO₄ is chemically stable in neutral and slightly basic media but it is not stable in strong acidic or basic media.^[10] Under illumination, it is not stable for photo-oxidation of water if it is not coupled with OECs.^[11] It appears that the slow interfacial hole transfer kinetics for water oxidation and the resulting hole accumulation at the BiVO₄/electrolyte interface results in anodic photocorrosion of BiVO₄. However, when BiVO₄ is covered with appropriate OECs or hole acceptors with fast oxidation kinetics are introduced to the electrolyte, anodic photocorrosion of BiVO₄ can be effectively suppressed.^[11,12]
5. Complete water splitting to H₂ and O₂ by BiVO₄
Since the CB edge of BiVO₄ is located just short of the thermodynamic level for H₂, BiVO₄ alone cannot produce H₂. Therefore, application of an external bias (e.g., coupling with a PV unit) or formation of a photoelectrochemical diode by combining an n-type BiVO₄ photoanode with a proper p-type semiconductor (photocathode) is necessary. Since the CB edge of BiVO₄ is already very close to the reduction potential of H₂, composition tuning of BiVO₄ to shift the CB edge position to the negative direction may also be possible.

Research Status

Significant advancement in the construction and understanding of efficient BiVO₄-based photoanode systems has been made within a short period of time owing to various newly developed ideas and approaches. The most frequently used synthesis methods to prepare BiVO₄ photoanodes include metal organic decomposition, chemical bath deposition, urea-precipitation method, hydrothermal synthesis, spray deposition, and electrochemical synthesis.^[1] During synthesis, various efforts to control morphology, formation of composite structures or heterojunctions, doping or composition tuning, and coupling with oxygen evolution catalysts (OECs) have been made. As a result, BiVO₄ currently shows the most promising performance for photo-oxidation of water in the low-bias region (< 0.6 V vs. RHE) among all oxide-based photoanodes studied to date.^[1]

Several theoretical studies have been performed to understand the optical and charge transport properties of BiVO₄ and also to identify the role of the dopants incorporated into the BiVO₄ structure. However, some controversies exist in these studies and the conduction mechanisms in BiVO₄ and doped BiVO₄ have not been thoroughly elucidated.

PEC White Papers: BiVO₄ for PEC hydrogen production

Approaches

Formation of Composite Structures Composite photoelectrodes where the main photon absorber is combined with an additional semiconductor or a conductor are often constructed to enhance the overall photon absorption, electron-hole separation, or charge transport processes. BiVO₄ has been most frequently coupled with WO₃ to form heterojunction structures in order to improve electron-hole separation. Rapid electron injection from the CB of BiVO₄ to the CB of WO₃, which is located at a more positive potential, can physically separate electrons from holes in the VB of BiVO₄ and may effectively reduce their recombination.^[13-17] Another interesting composite structure is a BiVO₄/SnO₂ electrode where a thin SnO₂ layer (*ca.* 10 nm) is placed between BiVO₄ and the FTO substrate.^[9,18] A significant enhancement in IPCE was observed because the SnO₂ layer with a very positive VB edge acts as a hole mirror, meaning holes are “reflected” at the SnO₂/BiVO₄ junction, presumably preventing electron-hole recombination at the FTO-related defect states. Without the SnO₂ layer, FTO-related defect states formed at the FTO/BiVO₄ interface act as recombination centers. More recently, BiVO₄/SnO₂/WO₃ multi-composite electrodes were also prepared,^[16] which demonstrated that the photocurrent observed from BiVO₄ was increased by adding a WO₃ layer under the BiVO₄ film. The photocurrent was further increased when a very thin SnO₂ layer was inserted between BiVO₄ and WO₃. To achieve complete water splitting with BiVO₄ in a cost-effective manner, monolithic composite tandem structures with an integrated PV cell should be explored. The BiVO₄ would effectively protect the underlying PV junction against photocorrosion, which is a problem for devices that are entirely based on III-V materials.^[19] Alternatively, BiVO₄ can be deposited on top of a smaller-bandgap n-type semiconductor to form a n-n heterojunction, in a similar manner as recently demonstrated for Fe₂O₃.^[20]

Doping Studies The most effective dopants identified to date, which increase the carrier concentration and photoelectrochemical performance of BiVO₄, are Mo⁶⁺ and W⁶⁺ ions that substitutionally replace V⁵⁺ ions.^[21-24] No changes in bandgap by Mo or W doping were observed while the increase in carrier density was confirmed by the decrease in the slope of Mott-Schottky plots. The results of the first-principles density-functional theory (DFT) calculations, which assumed substitutional replacement of V by Mo and W, showed that W and Mo serve as shallow donors and can effectively increase the carrier density in BiVO₄.^[23] Non-metal element, P, was also doped into BiVO₄ by the urea-precipitation method where PO₄³⁻ oxoanions were added as a P precursor to replace a small fraction of VO₄³⁻ oxoanions in the precursor solution.^[25] The EIS measurements suggested that the presence of P lowered the charge transfer resistance of BiVO₄ remarkably.

Coupling with Oxygen Evolution Catalysts In order to improve slow hole transfer kinetics of BiVO₄ for water oxidation, BiVO₄ have been coupled with various OECs (e.g. IrO_x, Co₃O₄, Co-Pi, and Pt).^[1] The most commonly used OEC to improve water oxidation kinetics of BiVO₄ or doped BiVO₄ photoanodes has been Co-Pi. Some studies compared electrodeposition and photodeposition (or photoassisted electrodeposition) of Co-Pi OEC onto the BiVO₄ photoanodes and found that BiVO₄/Co-Pi OEC prepared by photodeposition showed a superior performance for water oxidation.^[26-28] Recently, FeOOH was also identified as an efficient OEC that can work very well with BiVO₄.^[11,12] A few studies noted that the performance of a given OEC varies significantly depending on the type and the synthesis method used to prepare the photoanode.^[1] This suggests that the overall performance of a photoanode/OEC is significantly governed by the photoanode/OEC interface and, therefore, better understanding of this interface is necessary for further optimization of photoanode/OEC junctions.

Morphology Control When a semiconductor material is produced as a polycrystalline electrode, morphological details of the electrode such as size, shape and connectivity of the particles have a significant impact on the interfacial energetics, kinetics and charge transport properties.^[29] Therefore, understanding and controlling the morphological aspects of polycrystalline BiVO₄ electrodes provides an

PEC White Papers: BiVO₄ for PEC hydrogen production

effective way to enhance its photoelectrochemical properties. Atomic plane-dependent photoelectrochemical properties of powder type-BiVO₄ photocatalysts have been reported,^[1,30] suggesting that precise morphology control of BiVO₄ electrodes may also be advantageous. Also, construction of high surface area BiVO₄ electrodes that will increase the volume of space-charge region and enhance electron-hole separation is another effective way to increase the efficiencies of BiVO₄ photoanodes.

References

1. Y. Park, K. J. McDonald and K.-S. Choi, *Chem. Soc. Rev.*, 2013, **42**, 2321.
2. A. Kudo, K. Ueda, H. Kato and I. Mikami, *Catal. Lett.*, 1998, **53**, 229.
3. B. Xie, H. Zhang, P. Cai, R. Qiu and Y. Xiong, *Chemosphere*, 2006, **63**, 956.
4. M. G. Walter, E. L. Warren, J. R. McKone, S. W. Boettcher, Q. Mi, E. A. Santori and N. S. Lewis, *Chem. Rev.*, 2010, **110**, 6446.
5. T. Bak, J. Nowotny, M. Rekas and C. C. Sorrell, *Int. J. Hydrogen Energy*, 2002, **27**, 991.
6. A. Walsh, Y. Yan, M. N. Huda, M. M. Al-Jassim and S.-H. Wei, *Chem. Mater.*, 2009, **21**, 547.
7. A. Kudo, K. Omori and H. Kato, *J. Am. Chem. Soc.*, 1999, **121**, 11459.
8. D. K. Zhong, S. Choi and D. R. Gamelin, *J. Am. Chem. Soc.*, 2011, **133**, 18370.
9. F. F. Abdi and R. van de Krol, *J. Phys. Chem. C*, 2012, **116**, 9398.
10. F. F. Abdi, N. Firet, A. Dabirian and R. van de Krol. *Mater. Res. Soc. Symp. Proc.* 2012, **1446**, DOI: 10.1557/opl.2012.811.
11. J. A. Seabold and K.-S. Choi, *J. Am. Chem. Soc.*, 2012, **134**, 2186.
12. K. J. McDonald and Choi, K.-S., *Energy Environ. Sci.*, 2012, **5**, 8553.
13. J. Su, L. Guo, N. Bao and C. A. Grimes, *Nano lett.*, 2011, **11**, 1928.
14. P. Chatchai, Y. Murakami, S.-y. Kishioka, A. Y. Nosaka and Y. Nosaka, *Electrochim. Acta*, 2009, **54**, 1147.
15. S. J. Hong, S. Lee, J. S. Jang and J. S. Lee, *Energy Environ. Sci.*, 2011, **4**, 1781.
16. R. Saito, Y. Miseki and K. Sayama, *Chem. Commun.*, 2012, **48**, 3833.
17. K. Zhang, X.-J. Shi, J. K. Kim and J. H. Park, *Phys. Chem. Chem. Phys.*, 2012, **14**, 11119.
18. Y. Liang, T. Tsubota, L. P. A. Mooij and R. van de Krol, *J. Phys. Chem. C*, 2011, **115**, 17594.
19. O. Khaselev and J. Turner, *Science*, 1998, **280**, 425.
20. M.T. Mayer, C. Du, and D. Wang, *J. Am. Chem. Soc.*, 2012, **134**, 12406.
21. H. Ye, J. Lee, J. S. Jang and A. J. Bard, *J. Phys. Chem. C*, 2010, **114**, 13322.
22. W. Luo, Z. Yang, Z. Li, J. Zhang, J. Liu, Z. Zhao, Z. Wang, S. Yan, T. Yu and Z. Zou, *Energy Environ. Sci.*, 2011, **4**, 4046.
23. H. S. Park, K. E. Kweon, H. Ye, E. Paek, G. S. Hwang and A. J. Bard, *J. Phys. Chem. C*, 2011, **115**, 17870.
24. S. P. Berglund, A. J. E. Rettie, S. Hoang and C. B. Mullins, *Phys. Chem. Chem. Phys.*, 2012, **14**, 7065.
25. W. J. Jo, J.-W. Jang, K.-j. Kong, H. J. Kang, J. Y. Kim, H. Jun, K. P. S. Parmar and J. S. Lee, *Angew. Chem. Int. Ed.*, 2012, **51**, 3147.
26. S. K. Pilli, T. E. Furtak, L. D. Brown, T. G. Deutsch, J. A. Turner and A. M. Herring, *Energy Environ. Sci.*, 2011, **4**, 5028.
27. S. K. Pilli, T. G. Deutsch, T. E. Furtak, J. A. Turner, L. D. Brown and A. M. Herring, *Phys. Chem. Chem. Phys.*, 2012, **14**, 7032.

PEC White Papers: BiVO_4 for PEC hydrogen production

28. T. H. Jeon, W. Choi and H. Park, *Phys. Chem. Chem. Phys.*, 2011, **13**, 21392.
29. K.-S. Choi, *J. Phys. Chem. Lett.*, 2010, **1**, 2244.
30. G. Xi and J. Ye, *Chem. Commun.*, 2010, **46**, 1893.

PEC White Papers: Hematite for PEC hydrogen production

Hematite (α -Fe₂O₃) as a Photoelectrode for Photoelectrochemical Hydrogen Production

Heli Wang, National Renewable Energy Laboratory

Isabell Thomann, Rice University

Arnold J. Forman, Stanford University

Yat Li, University of California at Santa Cruz

Mahendra Sunkara, University of Louisville

Moreno de Respinis, Delft University of Technology

1. Introduction

The photoelectrochemical (PEC) production of hydrogen and oxygen, via water splitting reactions with photo-generated electrons and holes, was first demonstrated by Fujishima and Honda at a chemically biased TiO₂ with ultraviolet (UV) light.¹ Hematite (α -Fe₂O₃) has several advantages over other semiconductor materials for this purpose. With a band gap around 2 eV,^{2,3} it could utilize 40% of the incident solar spectrum. It has an excellent chemical stability in a broad pH range³ and its valence band (VB) is appropriate for the oxygen evolution reaction (OER).²⁻⁴ Moreover, it is abundant on earth, low in cost, and non-toxic making hematite an attractive candidate for PEC water splitting. Thus, it was investigated extensively in the late 70's and early 80's,⁴⁻⁹ mostly in the form of bulk, non-textured electrodes.

2. Technical Challenges and Research Status

Despite being one of the few promising materials for large-scale solar hydrogen production, hematite presents a number of challenges for application in PEC water splitting.

2.1 Energetic mis-match

First, like many *n*-type oxides, the conduction band (CB) of iron oxide lies 0.2 - 0.4 eV positive of the hydrogen evolution reaction (HER),³ meaning that an external bias is needed to drive this reaction, which reduces the overall efficiency. One way to provide this bias is via a multijunction device,¹⁰ in which the bottom photovoltaic (PV) cell/layer provides the necessary bias for the top PEC layer to drive the water splitting reactions.¹⁰⁻¹³ Such a bias can also be provided by combining two photoelectrodes in series, one *n*-type and one *p*-type.¹⁴⁻¹⁷ This dual-electrode configuration separates OER to the *n*- and HER to the *p*-type photoelectrodes, respectively, increasing the number of candidate semiconductors that could be used to build a stand-alone solar water splitting device.¹⁶ Alternatively, monolithic devices can be based on a photoanode biased with an integrated *p-n* junction.¹⁸ A promising approach consists of an *n-n* heterojunction PEC device in which a photoanode is deposited onto an *n*-type semiconductor that boosts the energy of the electrons.¹⁸⁻²¹ An alternate strategy to improve the band edge alignment is via modifications of the semiconductor surface, either with a pH-insensitive group, producing a surface dipole that is independent of pH, or by introducing a desired surface dipole/charge (see e.g. [Ref Lewis doi 10.1021/cr1002326]). Another possible way to shift the band edge up would be via quantum confinement.²² A 0.3-0.6 eV CB shift due to the quantum confinement effect could potentially locate the conduction band of hematite above the HER energy.

PEC White Papers: Hematite for PEC hydrogen production

2.2 Poor photo-response

It is generally accepted that the following are reasons for the poor photo-response of hematite:

- (1) Very short minority carrier (hole) diffusion length;⁴
- (2) High resistivity;
- (3) Low electron mobility and high recombination rate of photo-generated charge carriers.^{4,6}
- (4) Low visible light absorption coefficient

Since these effects are all inter-related, but difficult to probe quantitatively or remediate synthetically, the mechanisms and processes responsible for the low photo-response of hematite are far from being clearly understood. A deeper understanding of the semiconducting properties of the material is certainly needed for improvement. Different approaches, including various doping and alloying schemes^{3,7-9} have been attempted to increase the photo-response of iron oxide. As a result, significant progress in photo-response has been made recently by the research community.

2.2.1 Short hole diffusion length

For hematite, the minority carrier (hole) diffusion length is <10 nm, resulting in very inefficient carrier extraction. The recent development of high surface-area nanomaterials opens up new opportunities in overcoming this limitation from a structural design perspective. Nanostructured hematite photoanodes provide a much shorter diffusion path for minority carriers to reach the hematite/electrolyte interface, which can result in increased carrier collection efficiencies as has been observed in nanostructured hematite particle thin films.²³ Thin films based on oriented nanorod arrays²⁴⁻²⁷ also enhance the photogenerated carrier transport along the nanorods due to fewer grain boundaries (possible recombination centers) and a directed electron movement toward the back contact. The diameter of bundled ultrafine hematite nanorods is typically 4-5 nm,^{22,24-26} comparable to the hole diffusion length in hematite. Recently, several research groups have significantly improved the photo-response of hematite where a few milliamps/cm² of photocurrent density were obtained at 1.23 V_{RHE} with nanostructured thin films.^{21,28-36}

2.2.2 High resistivity

Poor electrical conductivity is another major hurdle for hematite. Elemental doping has been demonstrated to be a promising method to potentially address this limitation by significantly enhancing hematite's donor density.^{28,29,37,38} The development of performance-enhancing doping strategies has recently attracted a lot of attention.^{3,34,38-41} For example, Si-doping has been developed by spray pyrolysis and atmospheric pressure chemical vapor deposition techniques.^{21,28,29,37} The Si-doped hematite nanostructures achieved a photocurrent of 2.3 mA/cm² at 1.23 V_{RHE}, without the aid of a cocatalyst.²⁹ Sn-doped hematite, which can be achieved through Sn diffusion from an FTO substrate induced by thermal treatment or intentionally mixing the iron with Sn precursor during hydrothermal growth, has recently shown substantially improved PEC performance.^{30,31,35,42} Moreover, Ti-doping can enhance the donor

PEC White Papers: Hematite for PEC hydrogen production

density of mesoporous hematite film by nearly two orders of magnitude, resulting in a two-fold enhancement of photocurrent as compared to undoped films.⁴³

To further improve hematite electrodes, general strategies to understand the limiting factors for conductivity and photo-activity which are dominated by processes operating on the nanoscale (both in the bulk and at surfaces) are still required. Furthermore synthetic methods for forming suitable thin films with controllable composition, doping and proper structures, to optimize photocurrent and to cathodically shift the photocurrent onset potentials are required.

2.2.3 Recombination

A high charge carrier recombination rate is considered to be due to inefficient carrier diffusion and slow water oxidation kinetics at the hematite/electrolyte interface. One method addressing the recombination found in poor crystalline quality materials is to apply an ultra-thin single crystal hematite film on highly conductive TiSi₂ nanonets.³⁶ The thin layers facilitate charge transport to the back contact, minimize recombination at crystal defects and grain boundaries and reduce diffusion distances for charge carriers. It was reported that the absorbed photon conversion efficiency is almost the same as the incident-photon-to-electron conversion efficiency (IPCE), indicating excellent efficiency of charge separation and collection (quantum yield).

While nanostructuring is likely needed to reduce carrier path lengths to catalytic surfaces, it will be necessary to optimize carrier dynamics in these nanostructured materials for reduced recombination.⁴⁴⁻⁴⁶ This will require strategic modification of the hematite surface to minimize catalytic overpotentials (addition of co-catalysts) and to eliminate surface traps/defects.⁴⁷⁻⁴⁹ For example, an IrO₂ co-catalyst substantially shifted the photocurrent onset potential of Si-doped hematite to a more negative potential. Other oxygen evolution catalysts such as cobalt ions and cobalt phosphate have also been developed for PEC water oxidation at hematite.^{29,50}

2.2.4 Low absorption coefficient

If accompanied by high visible light absorption, the short minority carrier diffusion length would not be a major challenge. Unfortunately, being an indirect band-gap semiconductor, hematite is a relatively weak absorber of near band-gap photons (~0.1-1 μm absorption length in the 500-600 nm range),⁵¹ resulting in challenges for the optical design of the photoelectrode structures. In particular, novel strategies are required to increase the IPCE near the band-edge, and to improve light management and concentration in thin hematite films. One promising strategy may be the application of metallic plasmonic nanostructures or nanoparticles interspersed within hematite thin films to boost the effective near band-edge absorption.⁵¹ Such a strategy can help to alleviate the large mismatch between the length scales of absorption and carrier extraction. This could be done by confining incident sunlight close to the semiconductor/liquid interface, where the space charge layer can promptly separate the photocarriers, and thereby reducing recombination.⁵² Plasmon-enhanced photocatalytic activity of hematite has already proven successful with Au, Ag and Cu nanoparticles.⁵¹⁻⁵³

2.3 (Photo)Corrosion under extended operation conditions

PEC White Papers: Hematite for PEC hydrogen production

In terms of the practical application of hematite photoelectrodes for scalable solar hydrogen production, an improved understanding of extended operational stability will be required. It may be necessary to develop protective, corrosion resistant coatings which also permit charge transfer to solid/electrolyte interface.

Moreover, facile and large-scale production methods will be needed for hematite films^{27,38,54} and nanophotonic enhancement structures.⁵⁵ Substrate materials may be optimized to achieve a good ohmic contact for majority carrier extraction. If metal nanoparticles are to be used for photon management in large-scale applications, non-precious metals group (n-PMG) materials will be needed, calling for novel strategies to improve their corrosion stability.

3. Approaches

While different strategies have been explored to overcome the limitations inherent to hematite photoanodes and encouraging progress has been made, further research is clearly needed to better understand the fundamental properties and processes of nanostructured hematite and limiting factors. The complex nature of the system requires combined experimental and theoretical studies at an advanced level. Moreover, feasible approaches should focus on:

- Fundamental properties of both pristine and doped hematite; Nanostructured arrays and extremely thin film absorbers (ETA);²⁹ Limiting factors for conductivity and photo-activity;
- Surface chemistry at the nano-scale, including defects and/or oxygen vacancies; Charge generation, carrier extraction and electrochemical reactions;
- Suitable catalysts for fast water oxidation kinetics at the nanostructured hematite/electrolyte interface and reduced recombination;
- Optimizing the electromagnetic properties of photoelectrode structures for improved light management and concentration; modifying optical absorption in thin absorber structures (iterative computational-experimental strategies);
- Synthetic methods for forming suitable thin films, with controllable composition, doping and proper structures; Proper substrate – film interface for large scale fabrication;
- Modeling of photoelectrochemical process at nanostructured hematite; The influence of (nanoscale) structure on carrier generation, extraction and chemical reaction kinetics (modeling and experiments, e.g. time-resolved optical spectroscopies).

References

1. A. Fujishima and K. Honda, *Nature*, **238**, 37 (1972).
2. M. Grätzel, *Nature*, **414**, 338 (2001).
3. Y-S. Hu, A. Kleiman-Shwarstein, A. J. Forman, D. Hazen, J-N Park and E. W. McFarland, *Chem. Mater.*, **20**, 3803 (2008).
4. J. H. Kennedy and K. W. Frese, Jr., *J. Electrochem. Soc.*, **125**, 709 (1978).
5. R. A. Fredlein and A. J. Bard, *J. Electrochem. Soc.*, **126**, 1892 (1979).
6. M. P. Dare-Edwards, J. B. Goodenough, A. Hamnett and P. R. Trevellick, *J. Chem. Soc. Faraday Trans. 1*, **79**, 2027(1983).

PEC White Papers: Hematite for PEC hydrogen production

7. J. H. Kennedy and M. Anderman, *J. Electrochem. Soc.*, **130**, 848 (1983).
8. C. Leygraf, M. Hendewerk and G. Somorjai, *J. Solid State Chem.*, **48**, 357 (1983).
9. J. E. Turner, M. Hendewerk, J. Parmeter, D. Neiman, G. A. Somorjai, *J. Electrochem. Soc.*, **131**, 1777 (1984).
10. E. L. Miller, R. E. Rocheleau, X. M. Deng, *Int. J. Hydrogen Energy*, **28**, 615 (2003).
11. E. L. Miller, D. Paluselli, B. Marsen, R. E. Rocheleau, *Solar Energy Mat. Solar Cells*, **88**, 131 (2005).
12. O. Khaselev and J. A. Turner, *Science*, **280**, 425 (1998).
13. A. J. Bard and M. A. Fox, *Acc. Chem. Res.*, **28**, 141 (1995).
14. A. J. Nozik, *Appl. Phys. Lett.*, **30**, 567 (1977).
15. R. Abe, T. Takata, H. Sugihara and K. Domen, *Chem. Commun.* 3829 (2005).
16. H. Wang, T. Deutsch and J. A. Turner, *J. Electrochem. Soc.*, **155**, F91 (2008).
17. H. Wang and J. A. Turner, *J. Electrochem. Soc.*, **157**, F173 (2010).
18. Van de Krol R., Gratzel M.; “Photoelectrochemical hydrogen production”, Springer (2012)
19. Saito R., Miseki Y., Sayama K.; *Chem. Commun.*, **48**, 3833 (2012).
20. Su J., Guo L., Bao N., Grimes C.A.; *Nano Lett.* **11**, 1928 (2011).
21. Sivula K., Le Formal F., and Gratzel M.; *Chem. Mater.* **21**, 2862 (2009).
22. Vayssieres, L.; Sathe, C.; Butorin, S. M.; Shuh, D. K.; Nordgren, J.; Guo, J. H., *Adv. Mater.* **2005**, 17, 2320-2323.
23. U. Björkstén, J. Moser and M. Grätzel, *Chem. Mater.*, **6**, 858 (1994).
24. N. Beermann, L. Vayssieres, S.-E. Lindquist and A. Hagfeldt, *J. Electrochem. Soc.*, **147**, 2456 (2000).
25. L. Vayssieres, N. Beermann, S.-E. Lindquist and A. Hagfeldt, *Chem. Mater.*, **13**, 233 (2001).
26. T. Lindgren, H. Wang, N. Beermann, L. Vayssieres, A. Hagfeldt, S.-E. Lindquist, *Sol. Energy Mater. Sol. Cells*, **71**, 231 (2002).
27. B. Chernomordik, H. B. Russell, U. Cvelbar, J. B. Jasinski, V. Kumar, T. Deutsch, and M. K. Sunkara, *Nanotechnology*, **23**, 194009 (2012).
28. I. Cesar, A. Kay, J. Matinez and M. Grätzel, *J. Am. Chem. Soc.*, **128**, 4582 (2006).
29. A. Kay, I. Cesar and M. Grätzel, *J. Am. Chem. Soc.*, **128**, 15714 (2006).
30. K. Sivula, R. Zboril, F. Le Formal, R. Robert, A. Weidenkaff, J. Tucek, J. Frydrych and M. Grätzel, *J. Am. Chem. Soc.*, **132**, 7436 (2010).
31. J. Brillet, M. Grätzel and K. Sivula, *Nano Lett.* **10**, 4155 (2010).
32. K. Sivula, F. Le Formal, and M. Grätzel, *ChemSusChem*, **4**, 432 (2011).
33. C. J. Sartoretti, M. Ulmann, B. D. Alexander, J. Augustynski, A. Weidenkaff, *Chem. Phys. Lett.*, **376**, 194 (2003).
34. C. J. Sartoretti, B. D. Alexander, R. Solarsko, I. A. Rutkowska, J. Augustynski, R. Cerny, *J. Phys. Chem. B*, **109**, 13685 (2005).
35. Y. Ling, G. Wang, D. A. Wheeler, J. Zhang and Y. Li, *Nano Lett.* **11**, 2119 (2011).
36. Y. Lin, S. Zhou, S. Sheehan and D. Wang, *J. Am. Chem. Soc.*, **133**, 2398 (2011).
37. I. Cesar, K. Sivula, A. Kay, R. Zboril and M. Gratzel, *J. Phys. Chem. C*, **113**, 772 (2009).
38. G. M. Wang, Y. C. Ling, D. A. Wheeler, K. E. N. George, K. Horsley, C. Heske, J. Z. Zhang and Y. Li, *Nano Lett.*, **11**, 3503 (2011).
39. Hu, Y.-S.; Kleiman-Shwarsctein, A.; Stucky, G. D.; McFarland, E. W. *Chem. Commun.* 2652 (2009).
40. Jang, J. S.; Lee, J.; Ye, H.; Fan, F.-R. F.; Bard, A. J. *J. Phys. Chem. C* **113**, 6719 (2009).

PEC White Papers: Hematite for PEC hydrogen production

41. H. Tang, M.A. Matin, H. Wang, T. Deutsch, M. Al-Jassim, J. Turner and Y. Yan, *J. Appl. Phys.* **110**, 123511 (2011).
42. M. A. Lukowski and S. Jin, *J. Phys. Chem. C*, **115**, 12388 (2011).
43. G M. Wang, Y. C. Ling, D. A. Wheeler, K. E. N. George, K. Horsley, C. Heske, J. Z. Zhang and Y. Li, *Nano Lett.*, **11**, 3503 (2011).
44. Pendlebury, S. R.; Barroso, M.; Cowan, A. J.; Sivula, K.; Tang, J.; Gratzel, M.; Klug, D.; Durrant, J. R. *Chem. Commun.*, **47**, 716 (2011).
45. Cowan, A. J.; Barnett, C. J.; Pendlebury, S. R.; Barroso, M.; Sivula, K.; Gratzel, M.; Durrant, J. R.; Klug, D. R. *J. Am. Chem. Soc.*, **133**, 10134 (2011).
46. Peter, L. M.; Wijayantha, K. G. U.; Tahir, A. A. *Faraday Discussions* **155**, 309 (2012).
47. Klahr, B.; Gimenez, S.; Fabregat-Santiago, F.; Hamann, T.; Bisquert, J. *J. Am. Chem. Soc.*, **134**, 4294 (2012).
48. Le Formal, F.; Tetreault, N.; Cornuz, M.; Moehl, T.; Gratzel, M.; Sivula, K. *Chem. Sci.* **2**, 737 (2011).
49. Spray, R. L.; McDonald, K. J.; Choi, K.-S. *J. Phys. Chem. C*, **115**, 3497 (2011).
50. D.K. Zhong, M. Cornuz, K. Sivula, M. Graetzel and D. R. Gamelin, *Energy Environ. Sci.*, **4**, 1759 (2011).
51. Thomann, I.; Pinaud, B. A.; Chen, Z.; Clemens, B. M.; Jaramillo, T. F.; Brongersma, M. L. *Nano Lett.* **11**, 3440 (2011).
52. Warren S.C., Thimsen E.; *Energy Environ. Sci.*, **5**, 5133 (2012).
53. Gao H., Liu C., Jeong H.E., Yang P.; *ACS Nano*, **6**, 234 (2012).
54. U. Cvelbar, Z. Chen, M.K. Sunkara, M. Mozetic, *Small*, **4**, 1610 (2008).
55. Polman, A.; Atwater, H. A. *Nat. Mater.* **11**, 174 (2012).

2012 PEC White Paper: Photovoltage of Hematite**Photovoltage of α -Fe₂O₃**

Shannon W. Boettcher, University of Oregon
Arnold J. Forman, Stanford University
Muhammad N. Huda, University of Texas at Arlington
Heli Wang, National Renewable Energy Laboratory

In order to split water without an external bias the photovoltage generated by a complete PEC system must exceed 1.23 V, the thermodynamic minimum.¹ In general, the photovoltage generated by a semiconductor under illumination is proportional to the logarithm of the ratio of photocurrent to the recombination current.² For high quality semiconductors such as Si or GaAs the attainable photovoltage under one sun illumination is typically about 0.4 V less than the semiconductor bandgap (though both cannot do the water splitting task due to un-suitable band gaps and issues of oxidation/corrosion). For α -Fe₂O₃, there are at least two important recombination pathways that limit the photovoltage output to, in optimized cases, near 0.6 V, roughly 1.5 V less than the 2.1 eV bandgap.³ In fact, the derivation of the dependency of photovoltage in reference 2 assumed Boltzman-type particle distribution, whereas in case of the highly correlated electrons (which results in high localizations) in the conduction band of α -Fe₂O₃ can make the situation even worse. The two recombination pathways can be broadly classified as (i) interface, and (ii) bulk recombinations.. However, the fundamental limitations of α -Fe₂O₃ can be traced to the lack of bulk photoelectron available for conduction.

The first recombination pathway is majority electron transfer across the electrostatic barrier at the electrode/electrolyte interface. This recombination mechanism could in principle be mitigated by shifting the band-edge positions of an α -Fe₂O₃ electrode by surface modification to increase the equilibrium band bending and hence retard recombination via forward majority carrier transport.

Bulk and depletion region recombination within the semiconductor are also critical. It is well-known that the low mobility of carriers in α -Fe₂O₃ leads to short collection lengths. Hamann has recently shown in controlled thin-film α -Fe₂O₃ model systems that minority holes are collected via drift over a \sim 6 nm portion of the depletion region where a large electric field exists,⁴ leading to large bulk recombination currents and low internal quantum efficiencies ($<$ 0.5) even in the best devices. These high bulk recombination rates are fundamentally related to the localized electronic structure of α -Fe₂O₃ which can be described as a charge-transfer insulator.⁵ In this type of insulators, the bulk electron effective mass is extremely high, and hence the immobility of electrons are manifested by large electron-hole recombinations after photoexcitations.

In general, there are two ways to improve transport of the bulk photocurrent of α -Fe₂O₃. As it is well known that the main conduction mechanism in α -Fe₂O₃ is by small polaronic effect, reduction of volume would somewhat improve the photocurrent.⁶ However, volume reduction by doping is minimal, and can increase the photocurrent minutely.⁵ The second way involves the significant modification of the conduction band. The conduction band minimum (CBM), composed of Fe 3d orbitals, is dispersionless. Modification of the conduction band by selective doping is a possibility.⁷ For example, it has been shown that Ti doping in α -Fe₂O₃ can modify the CBM and lower the band gap, though not much dispersion was obtained to lower the electron effective mass. However, the dopant states may simply add additional bands below or in the

2012 PEC White Paper: Photovoltage of Hematite

CBM of α -Fe₂O₃, rather than modifying it; for example, Sc doping in α -Fe₂O₃.⁷ An alternate approach would be to alloy the dopant materials with α -Fe₂O₃, in which case an overall crystal phase transition is a possibility. It remains a largely undiscovered area regarding the nature of these new phase-spaces and the possible electronic properties of these alloys. With selective alloy strategies, the local magnetic moments can also be destroyed or compensated, which is another manifestation of the electron localization in α -Fe₂O₃. This will effectively take α -Fe₂O₃ (with new alloy crystal phase) out of “charge transfer” insulator regime. Though very challenging, these new alloys signatures can be predicted by DFT and be synthesized in the lab.

An important area of basic α -Fe₂O₃ research will be to determine what the photovoltage limits are in appropriately modified systems with inhibited forward electron transfer and hence recombination currents dominated by bulk/depletion region processes. Strategies for minimizing forward electron recombination current should focus on increasing band-bending and selectively inhibiting the kinetics of this “back reaction” transfer to solution species which, for water splitting, occurs primarily in the form of oxygen reduction. The latter may be realized through hole-selective (electron blocking) contact layers,⁸ and/or addition of an appropriately selective catalyst.⁹ However, given the inherent materials limitations of the pure α -Fe₂O₃ electronic structure, it is a challenge to improve the photovoltages sufficiently for application as a single bandgap photoelectrode for photoelectrochemical water splitting with unbiased efficiencies in excess of 10%. It may still find a role in tandem or two-bandgap devices coupled to photoelectrodes which can provide the remainder of the photovoltage but its photocurrent must still be improved so as not to limit the overall device current.

References

1. Walter, M.; Warren, E.; McKone, J.; Boettcher, S. W.; Qixi, M.; Santori, L.; Lewis, N. S., Solar Water Splitting Cells. *Chem. Rev.* **2010**, *110* (10), 6446-6473.
2. Lewis, N. S., A Quantitative Investigation of the Open-Circuit Photovoltage of the Semiconductor Liquid Interface. *J. Electrochem. Soc.* **1984**, *131* (11), 2496-2503.
3. Klahr, B. M.; Hamann, T. W., Current and Voltage Limiting Processes in Thin Film Hematite Electrodes. *Journal of Physical Chemistry C* **2011**, *115* (16), 8393-8399.
4. Klahr, B. M.; Martinson, A. B. F.; Hamann, T. W., Photoelectrochemical Investigation of Ultrathin Film Iron Oxide Solar Cells Prepared by Atomic Layer Deposition. *Langmuir* **2011**, *27* (1), 461-468.
5. Huda, M. N.; Al-Jassim, M. M.; Turner, J. A., Mott insulators: An early selection criterion for materials for photoelectrochemical H₂ production. *J. Renew. Sustain. Energy* **2011**, *3* (5).
6. Kleiman-Shwarstein, A.; Huda, M. N.; Walsh, A.; Yan, Y. F.; Stucky, G. D.; Hu, Y. S.; Al-Jassim, M. M.; McFarland, E. W., Electrodeposited Aluminum-Doped alpha-Fe₂O₃ Photoelectrodes: Experiment and Theory. *Chemistry of Materials* **2010**, *22* (2), 510-517.
7. Huda, M. N.; Walsh, A.; Yan, Y. F.; Wei, S. H.; Al-Jassim, M. M., Electronic, structural, and magnetic effects of 3d transition metals in hematite. *Journal of Applied Physics* **2010**, *107* (12), 123712.
8. Bisquert J.; Cahen D.; Hodes G.; Ruhle S.; Zaban A., Physical Chemical Principles of Photovoltaic Conversion with Nanoparticulate, Mesoporous Dye-Sensitized Solar Cells. *J. Phys. Chem. B*, 2004, *108* (24), pp 8106–8118

2012 PEC White Paper: Photovoltage of Hematite

9. Gorlin Y.; Jaramillo T.; A Bifunctional Nonprecious Metal Catalyst for Oxygen Reduction and Water Oxidation. *J. Am. Chem. Soc.*, 2010, 132 (39), pp 13612–13614.

PEC White Paper: a-SiC for PEC Hydrogen Production**The viability of using amorphous silicon carbide (a-SiC) as a photoelectrode for PEC hydrogen production***Jian Hu^a, Feng Zhu^a, Ilvydas Matulionis^a**Nicolas Gaillard^b**Todd Deutsch^c, Heli Wang^c*^a MVSystems, Inc.^b Hawaii Natural Energy Institute^c National Renewable Energy Laboratory

Date: October 1, 2012

Revised: November 30, 2012

Revised: August 12, 2013

Overview

Water splitting using photoelectrochemical (PEC) devices based on hydrogenated amorphous silicon (a-Si:H or a-Si in short) thin films and its alloys has the potential for low-cost and efficient hydrogen production. In 1998, Rocheleau et al reported use of the a-Si triple junction solar cell in a photoelectrode cell which was similar to an integrated photovoltaic (PV)/electrolyzer system (no wires or cell interconnections), and a solar-to-hydrogen (STH) efficiency of 7.8% was achieved in basic electrolyte [1]. More recently, Reece et al reported the STH efficiencies of 4.7% for a wired configuration and 2.5% for a wireless configuration in such a photoelectrode system which can be operated in near-neutral pH conditions [2]. The photoelectrode system comprising the a-Si solar cell interfaced to hydrogen and oxygen-evolving catalysts is considered a scheme mimic the photosynthetic process within a leaf that converts the energy of sunlight into chemical energy by splitting water to produce O₂ and H₂ [2]. The main drawback of using a-Si thin films is its poor corrosion resistance in electrolyte. In the above scheme, in order to avoid the a-Si solar cells (and ITO layer) exposed to electrolyte directly and thus enhance the durability of the entire PEC cell, the HER or OER catalyst was needed to separate the a-Si solar cells and ITO layer from electrolyte.

Alternatively, one could use a “hybrid” photoelectrode scheme [3]. In this configuration, the a-Si photovoltaic junction is protected by a semiconductor that makes a photoelectrochemical junction which is more durable in electrolyte than a-Si. Because this layer is connected in series, it contributes additional voltage allowing for a tandem (instead of triple) a-Si solar cell to be used leading to possibly increased photocurrent depending on current-matching of the solid-state devices. In addition, fabrication of a-Si solar cells is simplified.

Using hydrogenated amorphous silicon carbide (a-SiC:H or a-SiC in short) as the photoelectrode adds extra advantages over conventional metal oxides. First, a-SiC is of a bandgap of 1.9~2.3 eV which can be readily tuned with alternation of C source gas during growth [4], allowing more photocurrent and hence increased STH efficiency. For a-SiC with a bandgap of ~2 eV, the maximum available photocurrent approaches ~15 mA/cm², leading potentially to an STH efficiency of ~18%. Secondly, incorporation of the C in the film should lead to an increase in the corrosion resistance compared to the use of conventional a-Si films [5]. Thirdly, a-SiC has been extensively studied over the last three decades due to its importance in thin film Si solar cells, for instance, it has been used as a p-type window layer in a-Si solar cells for over 20 years [5,6], or as the absorbing layer in a-SiC p-i-n solar cells [7-10]. The state-of-art device performance exhibited a conversion efficiency of ~7%, with J_{sc} ~13 mA/cm² and V_{oc} >0.9V [10]. This vast knowledge base accumulated in PV filed over last three decades should be very useful in

PEC White Paper: a-SiC for PEC Hydrogen Production

development of a-SiC photoelectrode for PEC hydrogen production. Finally, fabrication of a-SiC films is routinely prepared by the Plasma Enhanced Chemical Vapor Deposition (PECVD) technique at a low temperature of ≤ 200 °C, in contrast with its crystalline counterpart which usually requires a high growth temperatures (1000-2000 °C) [11,12]. Note that growth of a-SiC is identical to that for a-Si since both use the PECVD technique and can be deposited in a same system. This is a very attractive for mass-production of the hybrid PV/a-SiC photoelectrode devices in a cost-effective fashion.

Research Status

The fabrication of the a-SiC photoelectrode consisting of p-type and intrinsic SiC layers has been previously reported [13-17]. The a-SiC photoelectrode exhibits a photocurrent density of ~ 8 mA/cm² @ -1.5V (V vs. SCE). To eliminate the external biases, hybrid PV/PEC device comprising a-SiC photoelectrode and an a-Si tandem solar cell has been developed, as shown in Fig.1(a) [18-21]. This type of hybrid PEC cell exhibited maximum photocurrent density of ~ 5 mA/cm² at zero bias (2-electrode configuration using RuO₂ counter electrode as OER catalyst). In addition, the hybrid device of a-Si/a-SiC configuration exhibits durability of >500 hours when tested at a constant current of ~ -4 mA/cm² in a 0.25M H₂SO₄ electrolyte, as tested so far. Hydrogen production was observed in short-circuit condition.

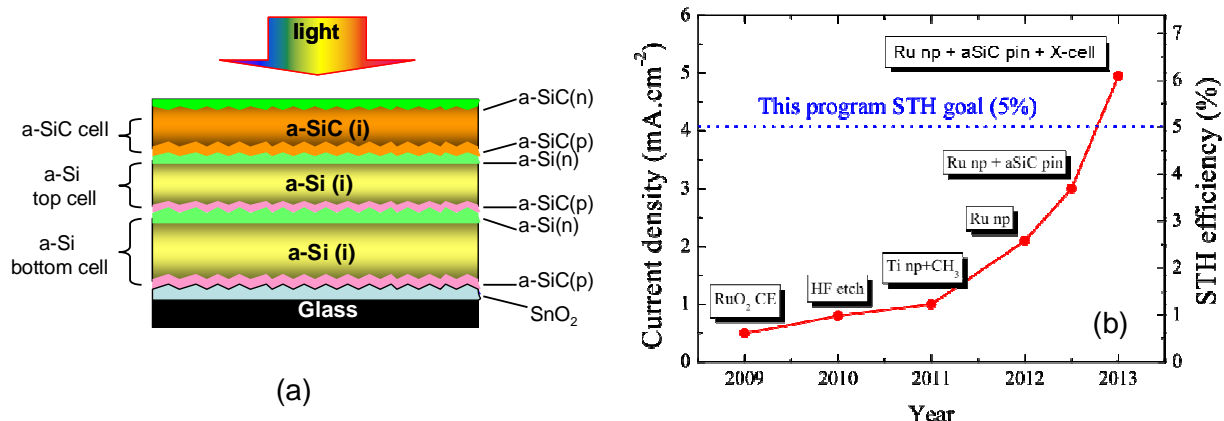


Fig.1. (a) Schematic diagram of the hybrid PV/a-SiC device. (b) Progress in improvement of the performance of the hybrid PV/a-SiC device¹.

Fig.1(b) shows yearly progress in improvement of the photocurrent current and the STH efficiency. We see that, with improved energetics and catalytic activity at the a-SiC/electrolyte interface using Ru nanoparticles treatment and enhanced performance of the photovoltaic solar cell, the short circuit photocurrent density increases to ~ 5 mA/cm², or equivalent to the STH efficiency of $\sim 6.1\%$. The performance of the hybrid PEC cells could be improved significantly once the PV cells and surface modification are further optimized. A-SiC as a photoelectrode makes possible an entirely a-SiC based hybrid PEC device, which could be produced in large quantities with lower cost using a cluster tool PECVD/Sputter system designed and fabricated at MVSystems, Inc.

Addressing the Challenges and Possible Solutions

1. Materials Efficiency

The poor interface between a-SiC and electrolyte was the main technical barrier, which resulted in a large over-potential loss and difficulty to extract charges at the interface. In order to minimize the surface barrier (i.e., partially caused by SiO_x native oxide) and increase STH efficiency, surface modification on

¹ For proprietary reason, the high performance PV device is termed as "X cell", whose details are not disclosed here.

PEC White Paper: a-SiC for PEC Hydrogen Production

a-SiC was necessary and has proven to be crucial to enhance the device performance. Over the past several years, several methods have been evaluated, including the HF etch, H₂ plasma treatment, thin a-SiNx and thin C-rich layer coverage by PECVD technique, CH₃-termination (methylation) or metal nanoparticles. The most promising technique so far is the surface treatment by low work function (WF) nanoparticles, which effectively reduces the onset potential and increases photocurrent from <1 mA/cm² to ~3 mA/cm² at zero potential measured at 2-electrode setup.

(1) Surface treatment by metal nanoparticles.

There are two key factors contributing to performance improvement of the hybrid device: a low Schottky barrier at a-SiC/metal interface, and catalytic property of the metal nanoparticles. For high work function metals (Pt, Pd and Au), the calculated barrier height is high, i.e., >1 eV; whereas for Ti, Ru and W with low WF, the barrier height is much lower. This difference in barrier height could partly explain why all low WF metal particles lowered overpotentials whereas all high WF metals increased them. In addition, although Ti exhibits a lower barrier height (0.39 eV) than that of Ru (0.77 eV), the latter usually leads to much higher photocurrent than the former at zero potential. One possibility is that Ru is of a better catalytic activity in hydrogen evolution than Ti. Yamada et al showed that, with Ru nanoparticles, the electron transfer from the photogenerated QuPh⁺NA to Ru nanoparticles results in hydrogen evolution even under basic conditions (pH10). In addition, the size of the Ru nanoparticles has effect on the catalytic reactivity for hydrogen evolution [22]. Similar behaviors such as size effect and hydrogen evolution in pH10 electrolyte were also observed for a-SiC [23].

In summary, with improved energetics and catalytic activity at the a-SiC/electrolyte interface using low WF Ru nanoparticles treatment, the overpotential loss is reduced to ~1.6V (@~3mA/cm²). This overpotential value is very close to ideal water splitting condition, i.e. ~1.5V. Further reduction in overpotential is expected by refining the Ru nanoparticles treatment, for instance, enhancing catalytic activity by applying Pt particles on Ru coated a-SiC photoelectrodes and hybrid devices. Meanwhile, cheaper low work function metals (e.g. W) were evaluated but more work is needed to establish its effectiveness.

(2) Modification of the a-SiC material properties.

It should be noted that C incorporation results in increase in disorder in a-SiC due to different bond lengths in C-C (1.54 Å) and Si-Si (2.24 Å) bonds [24], and increase of the density of states in the mid-gap region [25]. Deposition conditions such as substrate temperature, doping, type of source gases, RF power, pressure, etc, all affect a-SiC film properties. Generally the electronic quality of a-SiC is best at lower values of E_g (less than ~2.1eV) since the film is less defective. N-type and p-type doping can be achieved with good control of the Fermi level.

So far, bulk properties of a-SiC have not been altered. It is important to know that, like a-Si, a-SiC is by nature a weakly n-type semiconductor. The conductivity activation energy of intrinsic a-SiC, as measured at MVSsystems, is about 0.9 eV. By adding small amount of boron into the film, the Fermi energy (E_F) of intrinsic a-SiC will shift towards mid-gap, leading to a change in surface energy band structure. If assuming the surface E_F shifts downwards as in the bulk, the band alignment between the Fermi level and the O₂/H₂O redox potential would be improved. However, since the surface E_F is also critically affected by the surface states, which tends to pin the E_F, how much effect from doping in the intrinsic a-SiC is not known yet, and this will be determined by more experiments.

2. Materials Durability.

PEC White Paper: a-SiC for PEC Hydrogen Production

In the past, durability on hybrid PV/a-SiC device has been successfully demonstrated for up to 310 hours at a constant current density of -1 mA/cm^2 [26]. Recently, we have further achieved the durability of >500 hours on hybrid devices, under constant bias leading to a photocurrent density of $\sim 4\text{ mA/cm}^2$ in $0.25\text{M H}_2\text{SO}_4$ electrolyte.² This improvement in durability was due to contributions from several factors. The enhanced performance of the hybrid device, i.e., surface modification by the low work function metal nanoparticles (W nanoparticles were used in this test) allowed the device under test to sustain higher current biases. In addition, optimized process conditions for growing solid-state devices helped minimize defects. In fact, after about 700-hour test, no pinhole was found on the tested sample. Also, corrected testing procedure helped avoid interferences from handling and epoxy sealing. As a result, the yield and consistency of the durability test has been improved considerably. This result demonstrates that the a-SiC based hybrid device can be of good durability of >500 hours.

3. Device Configuration Designs.

Monolithically integrating a-SiC photoelectrode with Si solar cells is fairly straight forward, because both are fabricated using the same technique, PECVD, and at a similar low temperature of $\leq 200\text{ }^\circ\text{C}$. The key question here is how to maximize the performance (photocurrent and voltage) of the hybrid device through current match between the solar cell and photoelectrode. Table 1 shows the calculated performance of the hybrid devices where the solar cells and a-SiC layer is assumed to be in a good current match. Note that in case (1), where the hybrid PV/a-SiC device is of a-Si pin/pin/a-SiC pi configuration, the limiting factor is the a-Si tandem solar cell with a filtered photocurrent density of $\sim 6\text{ mA/cm}^2$ ³. Hence, the STH efficiency is limited as $\sim 7.6\%$. To reach this goal, in addition to improving the surface energetics as described previously (see “Materials Efficiency”), the possible approaches include:

- (1) Current match by optimizing thickness of each junction;
- (2) Using pin type configuration for the a-SiC photoelectrode;
- (3) To employ high performance solar cells.

In order to achieve current match, thickness of each intrinsic layer in the device was altered and tests were done using ITO as the top contact. As a result, the J_{sc} of $\sim 5.2\text{ mA/cm}^2$ was achieved due to better current matching. At 1.5V (practical water splitting bias), the photocurrent reaches $\sim 4.1\text{ mA/cm}^2$. When inserting an amorphous n⁺ layer ($\sim 10\text{nm}$ thick) underneath ITO, the barrier at a-SiC/ITO interface is eliminated. Thus a much better FF (0.65) was obtained. Another noticeable change in device performance was the increase of V_{oc} ($\sim 2.5\text{V}$), which is caused by a higher built-in electric field in a p-i-n configuration (compared with the p-i configuration). Further increase in J_{sc} is expected with optimized n⁺ layer properties.

In order to further enhance the STH efficiency beyond 10%, a more powerful solar cell engine must be used. One possible choice is outlined in Table 1.

² As of this writing the device under test has 700 hours, and is still operational. The test continues.

³ The a-SiC layer (100 nm thick) could generate maximum 8.8 mA/cm^2 photocurrent density, and the realistic operational current density (J_{ph}) is estimated as $\sim 7.6\text{ mA/cm}^2$, assuming $FF=0.75$ and the current density at the maximum power point is estimated by $\sqrt{FF} * J_{sc}$.

PEC White Paper: a-SiC for PEC Hydrogen Production

a-SiC Photoelectrode				PV devices			Hybrid
Configuration	E _g (eV)	J _{ph} (mA/cm ²) Available	Voc (V)	Configuration	J _{ph} (mA/cm ²) Filtered	Voc (V)	STH (%) possible
(1) p-i	2	7.66 (100nm)	0.5-0.6	a-Si/a-Si (620nm/132nm)	6.15	1.8-1.9	7.56
(2) p-i-n	2	12.4 (500nm)	>1		>25	>0.7	>12

Table 1. Calculated performance of the hybrid PV/a-SiC devices.

A conceptual configuration of a hybrid X cell/a-SiC device could be the one shown in Fig.2, where a-SiC photoelectrode (of pin structure) is integrated monolithically with the X cell. The combination of the novel X cell and the a-SiC pin cell could generate J_{sc} in a range of 14~17 mA/cm², or possible operational photocurrent density of 12.4~15 mA/cm² (assuming FF=0.8) equivalent to a STH efficiency of 15~18%.

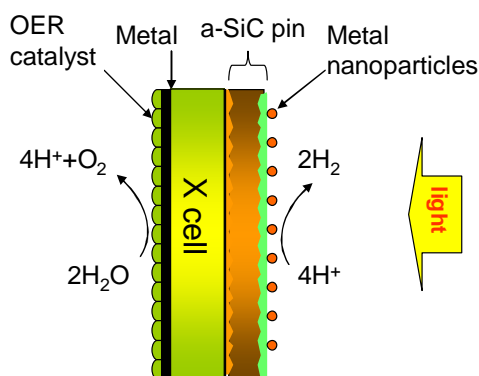


Fig.2. Schematic diagram for the hybrid X cell/a-SiC pin photoelectrode.

It should be noted that the triple junction solar cells as used in a photoelectrode system comprising the a-Si solar cell only [1-2], in spite of its high Voc (~2.2V), could only provide a limit operation current density, i.e., ~8.3 mA/cm² [27]. These solar cells thus are not suitable for achieving a STH efficiency of 11%.

Appendix: Current Matching in Multi-junction Solar Cells (A Review)

References

- [1] R. E. Rocheleau, E. L. Miller, and A. Misra, *Energy & Fuels* 1998, 12, 3-10
- [2] S. Y. Reece, J. A. Hamel, K. S. Thomas, D. Jarvi, A. J. Esswein, J. J. H. Pijpers, D. G. Nocera, *Science* 334, 645 (2011). References therein.
- [3] E. L. Miller; R. E. Rocheleau, S. Khan, *International Journal of Hydrogen Energy* 29 (2004) 907 – 914
- [4] Madan and Shaw, *The Physics and Applications of Amorphous Semiconductors*, Academic Press, San Diego (1989), p.155.

PEC White Paper: a-SiC for PEC Hydrogen Production

- [5] L. H. Hihara, A. Iwane, S. Voss, R. E. Rocheleau and Z. Zhang, *Corrosion Science*, 41, pp.1403 (1999)
- [6] Y. Tawada, H. Okamoto, Y. Hamakawa, *Appl. Phys. Lett.* 39(3) (1981), p. 237-239.
- [7] C. M. Fortmann, J. O'Dowd, J. Newton, and J. Fischer, *AIP Conference Proceedings*, Vol 157, pp. 103-110
- [8] R.E. Holli"sworth, P.K. Eulat and A. Mada, *Proc. 19th IEEE Photovoltaic Specialist Conference*, pp.684 (1987)
- [9] R. Platz, D. Fischer and A. Shah, "VHF-Ddposited a-SiC:H alloys for high-bandgap solar cells: Combining high Voc and reasonable stability", (1994)
- [10] F. Zhu, J. Hu, A. Kunrath, I. Matulionis, B. Marsen, B. Cole, E. Miller and A. Madana, *Proceedings of the SPIE - The International Society for Optical Engineering*, v 6650, n 1, p 66500S-1-9, 13 Sept. 2007
- [11] H. J. Davies, *Physics of Low-Dimensional semiconductors: an introduction*. Cambridge University Press, 1997.
- [12] F. Rinaldi, *Basics of Molecular Beam Epitaxy (MBE) - Annual Report. 2002*, Optoelectronics Department, University of Ulm.
- [13] A. Stavrides, A. Kunrath, J. Hu, R. Treglio, A. Feldman, B. Marsen, B. Cole, E. Miller, and A. Madan, *Proc. SPIE Solar Hydrogen and Nanotechnology*, Vol.6340 (2006).
- [14] F. Zhu, J. Hu, A. Kunrath, I. Matulionis,, A. Kunrath, B. Marsen, B. Cole, E. Miller, and A. Madan, *Proc. SPIE Solar Hydrogen and Nanotechnology II*, vol.6650 (2007).
- [15] I. Matulionis, F. Zhu, J. Hu, J. Gallon, A. Kunrath, E. Miller, B. Marsen, and A. Madan, *Proc. SPIE Solar Energy and Hydrogen*, vol.7044 (2008).
- [16] J. Hu, F. Zhu, I. Matulionis, A. Kunrath, T. Deutch, L. Kuritzky, E. Miller, and A. Madan, *Proc. 23rd European Photovoltaic Solar Energy Conference*, Valencia, Spain, 69 (2008).
- [17] F. Zhu, J. Hu, I. Matulionis, Todd Deutsch, Nicolas Gaillard, A. Kunrath, E. Miller and A. Madan, *Philosophic Magazine*, 89:28, (2009) 2723-2739.
- [18] J. Hu, I. Matulionis, F. Zhu, J. Gallon, T. Deutsch, N. Gaillard, A. Kunrath, E. Miller, and A. Madan, *Proc. MRS Meeting*, vol.1171, S03-05 (2009).
- [19] F. Zhu, J. Hu, I. Matulionis, T. Deutsch, N. Gaillard, E. Miller, and A. Madan, (book chapter) "Solar Energy", edited by: Radu D. Rugesu, ISBN 978-953-307-052-0, pp. 432, February 2010, INTECH,
- [20] F. Zhu, J. Hu, I. Matulionis, T. Deutsch, N. Gaillard, E. Miller, and A. Madan, presented at NHA hydrogen conference and Expo., Long beach, CA, May 3-6, 2010.
- [21] I. Matulionis, J. Hu, F. Zhu, J. Gallon, N. Gaillard, T. Deutsch, E. Miller, and A. Madan, *Proc. SPIE Solar Hydrogen and Nanotechnology V*, vol.7770 (2010).
- [22] Y. Yamada, et al, *J. Am. Chem. Soc.*, 2011, 133 (40), pp 16136-16145
- [23] N. Gaillard, Interim Report, December 14, 2011
- [24] M. P. Schmidt, et al, *Phil. Mag.* B51, 581 (1985)
- [25] A. Morimoto, et al, *Jap. J. Appl. Phys.*, 21, 2 (1982)
- [26] J. Hu, DOE AMR meeting, Washington DC, May, 2011
- [27] B. Yan, G. Yue, L. Sivec, J. Yang, and S. Guha, *Appl. Phys. Lett.* 99, 113512 (2011). This group reported the highest efficiency achieved by a triple junction Si thin film solar cell in a configuration of a-Si/a-SiGe/nc-Si, 16.3%, but with a limited Jsc of merely 9.4 mA/cm².

PEC White Paper Appendix on Current Matching

Appendix: Current Matching in Multi-junction Solar Cells –A Review

Table of Contents:

1. High efficiency in multi-junction solar cells.
2. Current matching in two-terminal multi-junction solar cells.
3. Effect of sub-cell bandgaps on current-matching.
4. Effect of top-cell thickness on current matching.
5. Current matching in a-Si based multi-junction solar cells.
6. Current matching in PEC devices.

1. High efficiency in multi-junction solar cells.

Multijunction solar cells provide a simple and straightforward way of overcoming the fundamental conversion efficiency limitation of the single junction solar cell [1]. The fundamental concept underlying multijunction solar cells is “spectrum splitting.” In this configuration, the top junction which is of the highest bandgap “filters” the sunlight to the bottom junction. Thus, only high-energy photons are absorbed in the top cell whereas photons with energy less than the top junction bandgap pass through towards the inner cells (or the bottom cell). This concept is illustrated in Fig.1, showing the solar spectrum (upper graph) divided up into two regions for conversion by a two-junction cell (lower graph). A larger open-circuit voltage (V_{oc}) across the top junction than that across the bottom cell is achieved due to a larger bandgap in the top cell, leading to more incident power conversion. This is the “spectrum-splitting” effect.

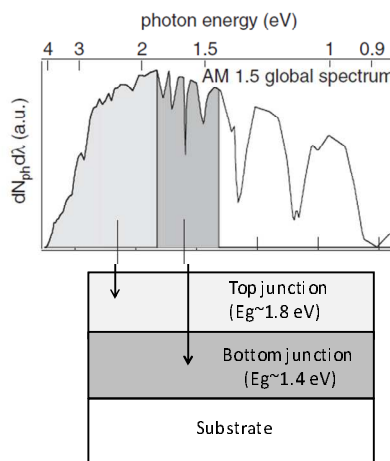


Fig.1. AM1.5 Global Spectrum and schematic of a two-junction solar cell with different bandgaps, (1.4 eV and 1.8 eV for the bottom and top cell), showing the spectral regions converted by each junction.

The thermodynamic efficiency limit of the multi-junction stack (with infinite number of cells) can be calculated based on the detailed recombination-generation balance equation as originally proposed by Shockley and Queisser, given by [2]

PEC White Paper Appendix on Current Matching

$$\eta = \frac{\int_0^{\infty} \eta_{mc}(\varepsilon) \dot{e}_s d\varepsilon}{\int_0^{\infty} \dot{e}_s d\varepsilon} = \frac{1}{\sigma_{SB} T_s^4} \int_0^{\infty} \eta_{mc}(\varepsilon) \dot{e}_s d\varepsilon = \frac{1}{\sigma_{SB} T_s^4} \int_0^{\infty} i(\varepsilon, V) V|_{\max} d\varepsilon$$

where $\eta_{mc}(\varepsilon)$ is the monochromatic cell efficiency, and $i(\varepsilon, V)$ is the current in a monochromatic cell. σ_{SB} ($= 5.67 \times 10^{-8} \text{ Wm}^{-2} \text{ K}^{-4}$) is the Stefan–Boltzmann constant. For $T_s = 6000 \text{ K}$ and $T_a = 300 \text{ K}$, the sun and ambient temperature, respectively, one finds an efficiency of 68.2% for 1 sun illumination intensity and 86.8% for 45900 suns intensity [2], the highest efficiency limit of known ideal photovoltaic converters and much higher than that of a single junction (31% for unconcentrated and 40.7% for concentrated solar cells [3]).

In practice, the efficiency of a multi-junction solar cell is much lower than the above theoretical value. So far, the highest efficiency achieved in a concentrated multi-junction solar cell was 44% (roughly half of the theoretical limit), as reported by Solar Junction (USA), using a monolithic two-terminal lattice matched triple junction cell of GaInP/GaAs/GaInNAs operating at a concentration factor of 947 suns [4]. In unconcentrated multi-junction solar cells, Sharp (Japan) recently reported the highest efficiency of 37.7% using an GaInP/GaAs/GaInAs triple junction configuration [5].

The difference between the actual cell efficiency and theoretical limit indicates much more efforts would be needed to reduce various losses and hence improve the performance of the multi-junction solar cells. These losses include reflection loss at the cell surface and various sub-cell interfaces, resistive loss at the sub-cell interfaces, current matching among sub-cells, etc. In the following, issues mainly related to the current-matching will be reviewed.

2. Current matching in two-terminal multi-junction solar cells.

A multi-junction solar cell can be constructed in different ways, depending on connection of power leads to the multijunction stack. For instance, for a two-subcell stack, there could be of a two-, three-, or four-terminal configuration. Among these, the two-terminal series-connected configuration provides truly monolithic, fewest possibilities for interconnection of the devices, requiring a simpler cell structure and processing. However, this configuration requires that the photocurrents of the subcells be closely matched, since in this series connection the subcell with the least photocurrent dictates the current generated by the entire device.

The current-voltage characteristics of the two-terminal series-connected m junction devices can be described by [6]

$$V(J) = \sum_{i=1}^m V_i(J);$$

where $V_i(J)$ is an individual $J-V$ curve the i th device. In order for each individual subcell to operate at its own maximum-power point, it is apparent that the maximum current density must be the same for all the subcells, i.e. $J_{mp,1} = J_{mp,2} = \dots = J_{mp,m}$. If this is the case, then the maximum power output of the combined multijunction device is the sum of the maximum power outputs of the subcells. Otherwise, if the subcells do not all have the same $J_{mp,i}$, some of the subcells will operate away from their maximum power points. As a result, the output power from the entire device will be reduced.

3. Effect of sub-cell bandgaps on current-matching.

PEC White Paper Appendix on Current Matching

For a cell with n junctions numbered from top to bottom as 1/2/.../n and with corresponding bandgaps $E_{g1}/E_{g2}/\dots/E_{gn}$, the short-circuit current density of the m th subcell is given by

$$J_{SC,m} = e \int_0^{\lambda_m} (1 - \exp[-\alpha_m(\lambda)x_m]) \Phi_m(\lambda) d\lambda,$$

where $\lambda_m = hc/E_{gm}$ is the wavelength corresponding to the bandgap of the m th subcell, and $\Phi_m(\lambda)$ the incident spectrum seen by the m th subcell. This equation shows that J_{SC} depends on the bandgaps of the various junctions. For instance, in the simple case of a two-junction cell, because the bottom junction is filtered by the top junction, the bottom-junction current density $J_{SC,2}$ depends on both E_{g1} and E_{g2} , whereas $J_{SC,1}$ depends only on E_{g1} . Fig.2 shows calculated $J_{sc,1}$ and $J_{sc,2}$ as a function of top cell bandgap for $E_{g2} = 1.42$ eV for the AM1.5 global spectrum [6].

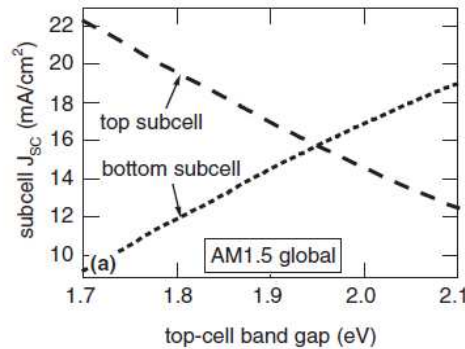


Fig.2 J_{SC1} and J_{SC2} as a function of top-subcell bandgap E_{g1} for a bottom-subcell bandgap $E_{g2} = 1.42$ eV.

The figure shows that as E_{g1} decreases, J_{SC1} increases and J_{SC2} decreases, becoming less than J_{SC1} for $E_{g1} < 1.95$ eV. The J_{SC} for the entire solar cell will be the lesser of J_{SC1} and J_{SC2} . This quantity is a maximum at the current-matched bandgap $E_{g2} = 1.95$ eV, and falls off rapidly as E_{g1} is decreased below 1.95 eV.

The current-matching constraint puts relatively tight constraints on the selection of bandgaps for the various junctions in this structure. The highest efficiency as mentioned previously, 68.2% (under 1 sun illumination) and 86.8% (under concentrated illumination), is obtained with an infinite number of solar cells, each one biased at its own voltage and illuminated with monochromatic radiation [2]. In the case of finite number of cells, many authors have calculated the optimal bandgap combination [7-11]. For a two-junction series-connected cell under 1 sun illumination, a maximum efficiency of 44.3% [8], 42% [2], 40.7% [9] and 38% [10] or 35% [11] was deduced for the optimum bandgap pairs of 1.0/1.8 eV, 1.0/1.9, 0.97/1.65 eV and 1.13/1.75 eV, respectively.

For the three-cell configuration, the above authors also reported the calculated 1-Sun efficiency in a range of 35 ~ 50% using various bandgap combinations: 35.6% with 1.1/1.55/2.5 eV [8], 50.3% with 1.0/1.6/2.2 eV [10] and 49% with 0.8/1.4/2.3 eV [2].

4. Effect of top-cell thickness on current matching.

Alternation of the top-cell thickness is a commonly used method for achieving current matching in fabrication of two-junction solar cells [12]. This is because the absorption coefficient for solar-cell materials is finite, and a cell of finite thickness will not absorb all the incident above-bandgap light. The thinner the cell, the greater the transmission (this is particularly true for photons near the bandgap where the absorption is very small). If, before thinning, J_{SC1} (top cell) $<$ J_{SC2} (bottom cell) then the top subcell can be thinned to make $J_{SC1} = J_{SC2}$. Although the actual current at the maximum power point is not same

PEC White Paper Appendix on Current Matching

as J_{sc} , this should be a very good approximation for high-quality, high-bandgap cells. A similar approach can be also applied to other multi-junction solar cells such as the triple junction stack, in order to achieve current matching. In this case, thickness of both the top sub-cell and the middle sub-cell is alternated for optimization.

5. Current matching in a-Si based multi-junction solar cells.

Amorphous silicon (a-Si in short) multijunction solar cells fabricated in a stacked structure is particularly successful both because there is no need for lattice matching, as is required for crystalline heterojunctions, and also because the bandgap is readily adjusted by alloying with Ge, C or by forming nanocrystallin silicon (nc-Si). Another added advantage is the improved stability in a-Si tandem solar cells compared with the a-Si single junction devices, since the former can utilize thinner intrinsic a-Si layers leading to reduced light-induced degradation. Finally, since a multijunction cell delivers its power at a higher operating voltage and lower operating current than a single-junction cell, the lower current reduces resistive losses. Higher solar conversion efficiency than single-junction cells has been achieved in multijunction, a-Si-based solar cells. Fig.3 shows schematic diagrams of a few a-Si multijunction configurations presently used in most commercial modules.

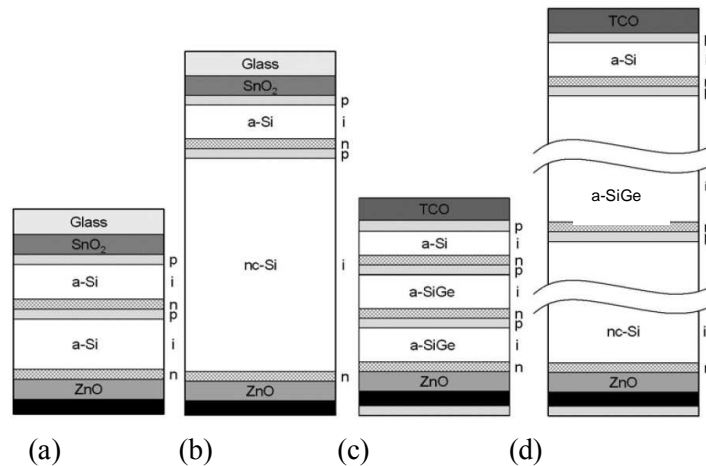


Fig.3 Schematic diagrams of some typical a-Si multijunction solar cells.

The a-Si/a-Si tandem solar cell (Fig.3(a)) was very first kind of a-Si based multi-junction devices developed. The highest efficiency so far reported in the a-Si/a-Si tandem solar cell is ~12% [13]. Compared with the a-Si single junction device, it exhibits not only increased efficiency, i.e., ~12% vs. ~10%, but also improved stability under illumination, i.e., degradation of $\leq 5\%$ vs. $>10\%$ in a first 100 hours test [14]. However, the performance of this type of tandem solar cell is limited by its bandgap since both junctions are of an identical bandgap (~1.75eV). Replacing the a-Si bottom sub-cell with a-SiGe ($E_g=1.4\sim 1.6$ eV) helps increase of the J_{sc} due to the spectrum splitting effect, leading to an improved efficiency of ~14% [15]. Compared with a-Si, a-SiGe is more defective. This limits the even higher performance of a-Si/a-SiGe tandem solar cells. A more promising approach is the “micromorph” tandem solar cell where a more stable nc-Si (Fig.3(b)) is used as the bottom sub-cell. Besides, since nc-Si is of a bandgap of ~1.1 eV, the a-Si/nc-Si pair is closer to optimum bandgap combination for achieving a high efficiency. The reported highest efficiency of a-Si/nc-Si tandem solar cells has reached 14.7% [16]. One of key techniques used in a-Si/nc-Si tandem devices is the introduction of a highly transparent tunneling junction between the a-Si top and nc-Si bottom sub-cells, which not only minimizes the series resistance, but also helps reflect more short-wavelength photons back into the a-Si layer, resulting in increased J_{sc} in the a-Si sub-cell and achieve better current matching with the nc-Si bottom sub-cell [17].

PEC White Paper Appendix on Current Matching

Further improvement in efficiency has been achieved using the triple junction configuration as shown in Figs.3(c) and (d). These triple junction devices, a-Si/a-SiGe/a-SiGe and a-Si/a-SiGe/nc-Si devices, fully make use of the spectrum splitting effect by utilizing three absorbing layers of different bandgaps (1.8/1.6/1.4 eV and 1.8/1.5/1.1 eV respectively), lead to an improved efficiency of 15.2% [18] and 16.3%, respectively [19].

6. Current matching in PEC devices.

Water splitting using photoelectrochemical (PEC) devices based on a-Si thin films and its alloys offers a potential low-cost and efficient hydrogen production approach. Currently, two different PEC schemes utilizing a-Si multi-junction solar cells have been explored. One is the use of the a-Si triple junction solar cell in a photoelectrode cell which is similar to an integrated photovoltaic (PV)/electrolyzer system (no wires or cell interconnections), and a solar-to-hydrogen (STH) efficiency of 7.8% was demonstrated in basic electrolyte [20]. An alternative scheme is a “hybrid” photoelectrode [21], where the a-Si photovoltaic junction is integrated with a semiconductor photoelectrode that makes a photoelectrochemical junction which is more durable in electrolyte than a-Si. Because this layer is connected in series with an a-Si multi-junction device, current-matching between the PV cell and photoelectrode is necessary in order to achieve a high STH efficiency (details of the hybrid device consisting of a-Si tandem cell/a-SiC photoelectrode is described in the main text).

Compared with the case of solid-state devices operating in the air, operation of the PEC device in electrolyte is more complicated, involving not only photovoltaic and optical, but also electrochemical phenomena. In order to analyze these behaviors, Miller et al [21] have developed integrated models comprising both a lumped-circuit model for a photocell (shown in the left-hand side of Fig.4(a)) and an electrochemical model for the current-dependent load (shown in the right-hand side of Fig. 4(a)), whose kinetics is determined by the Butler–Volmer equation. The current-dependent overpotential loss due to charge transfer at the electrode surface and additional potential drop due to ions transport through the electrolyte are included in this analysis. This one-dimensional model is able to capture the key physical and chemical nature of the PEC system.

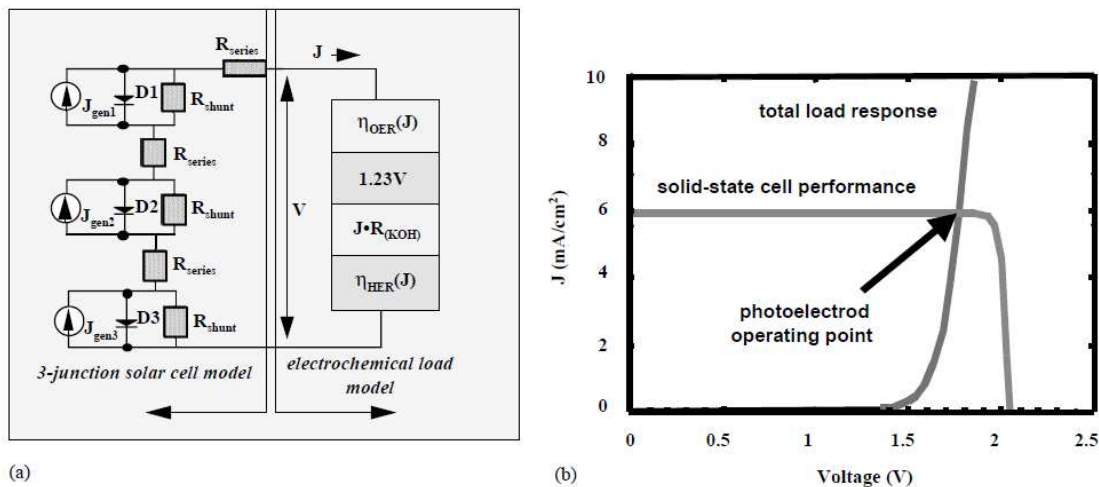


Fig.4 (a) Integrated models of triple-junction photoelectrode; (b) load-line analysis to determine photoelectrochemical operating point [21].

This analysis shows that the operating point for the PEC device is no longer depends only on the current-matching among individual sub-cells of the PV device, and will be determined by both the light J-V curve of the PV cell and the electrochemical load curve, or the intersection of these two curves as shown in Fig.4(b).

PEC White Paper Appendix on Current Matching

Reference

- [1] W. Shockley and H. Queisser, J. Appl. Phys. **32**, 510–519 (1961)
- [2] A. De Vos and H. Pauwels, Appl. Phys. **25**, 119–125 (1981)
- [3] A. Luque and A. Mart, “Theoretical Limits of Photovoltaic Conversion and New-generation Solar Cells” (Chapter 4), Handbook of Photovoltaic Science and Engineering, 2nd Ed. Edited by A. Luque and S. Hegedus, John Wiley & Sons, 2011. Reference therein.
- [4] Solar Junction (USA) news release, http://www.sj-solar.com/about_us/latest-news.php, October 15, 2012
- [5] Sharp (Japan) news release, <http://www.sharp-world.com/corporate/news/121205.html>, December 5, 2012
- [6] D. J. Friedman, J. M. Olson and S. Kurtz, “High-efficiency III–V Multijunction Solar Cells” (Chapter 8), Handbook of Photovoltaic Science and Engineering, 2nd Ed. Edited by A. Luque and S. Hegedus, John Wiley & Sons, 2011. Reference therein.
- [7] J. J. Loferski, Proc. 12th IEEE Photovoltaic Specialists Conference, 1976, p.957-961.
- [8] A. Bennett and L. C. Olsen, Proc. 13th IEEE Photovoltaic Specialists Conference, 1978, p. 868-873.
- [9] I. Tobias, A. Luque, Progress in Photovoltaics: Research and Applications **2002**, 10, 323–329
- [10] M. E. Nell and A. M. Barnett, IEEE Trans. Electron Devices ED-34 257 (1987).
- [11] F. Meillaud, A. Shah, C. Droz, E. Vallat-Sauvain, and C. Miazza, Solar Energy Materials & Solar Cells 90 (2006) 2952–2959
- [12] S. R. Kurtz, P. Faine, J. M. Olson, Journal of Applied Physics **1990**, 68, 1890
- [13] J. Yang, K. Lord, S. Guha and S.R. Ovshinsky, Mat. Res. Soc. Symp. Proc. Vol. 609, 2000
- [14] T.Yoshida, K.Maruyama, O.Nabeta, Y.Ichikawa, H.sakai and Y.Uchida, Proc. 19th IEEE Photovoltaic Specialists Conference, p.1095, 1987
- [15] X. Deng, Proc. 31st IEEE Photovoltaic Specialists Conference, p. 1365-1370, 2005
- [16] K.Yamamoto, A. Nakajima, M.Yoshimi, T. Sawada, S. Fukuda, T. Suezaki, M. Ichikawa, Y. Koi, M. Goto, T. Meguro, T. Matsuda, M. Kondo, T. Sasaki, Y. Tawada, Solar Energy, **77**, 939(2004)
- [17] D. Fischer, S. Dubail, J. A. Anna S&an, N. Pellaton Vaucher, R. PI&z, Ch. Hof, U. Kroll, J. M&r, P. Tomes, H. Keppner, N. Wyrsh, M. Go&, A. Shah, and K-D.Ufert, Proc. 25th IEEE Photovoltaic Specialists Conference, 1996, p. 1053
- [18] J. Yang, A. Banerjee, K. Lord, S. Guha, 2nd World Conf. On Photovoltaic Energy Conversion, 387 (1998)
- [19] B. Yan, G. Yue, L. Sivec, J. Yang, and S. Guha, Appl. Phys. Lett. 99, 113512 (2011)
- [20] R. E. Rocheleau, E. L. Miller, and A. Misra, Energy & Fuels 1998, 12, 3-10
- [21] E. L. Miller; R. E. Rocheleau, S. Khan, International Journal of Hydrogen Energy 29 (2004) 907 – 914

PEC White Paper Appendix on Energetic Mismatch

Energetic Mismatch

*Heli Wang, National Renewable Energy Laboratory
Arnold J. Forman, Stanford University
Moreno de Respinis, Delft University of Technology
Nicolas Gaillard, Hawaii Natural Energy Institute
Shannon Boettcher, University of Oregon*

Energetic mismatch is a major challenge for most semiconductors studied for PEC water splitting. For water splitting to occur using a single semiconductor photoelectrode, the semiconductor conduction band minima (CBM) must be more negative of the hydrogen evolution reaction (HER) and valence band maxima (VBM) more positive of the oxygen evolution reaction (OER), respectively.¹⁻³ If these criteria are not met, the equilibrium band bending will not be sufficient for the semiconductor to generate a quasi-Fermi level splitting greater than 1.23 V, the thermodynamic minimum needed for photoelectrochemical water splitting.^{3b}

Although some wide band-gap materials satisfy this criterion (e.g. SrTiO₃), this is at the expense of charge carrier generation, as only a small fraction of the solar spectrum is absorbed. This leads to very low water splitting efficiencies.

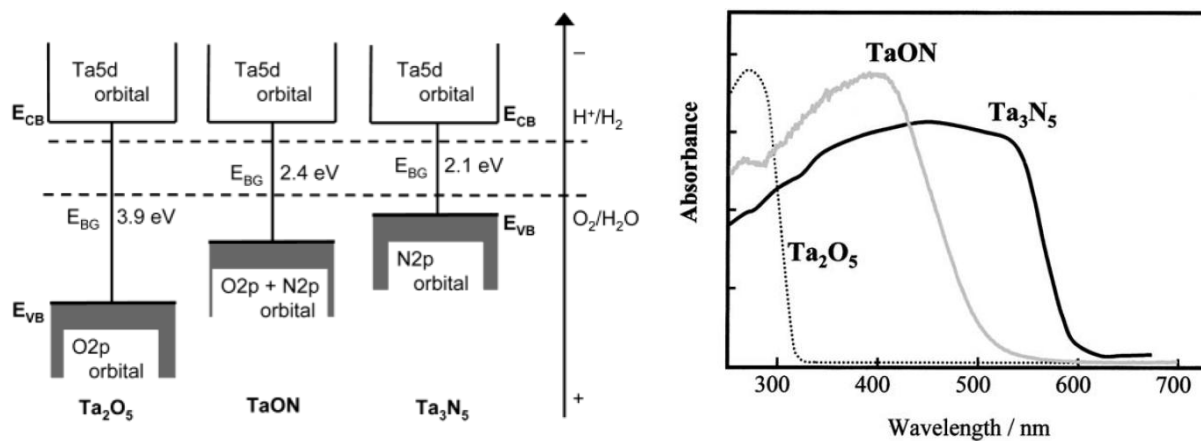


Figure 1. a) Band diagram of Ta oxide-oxynitride-nitride (left figure), and b) their optical absorbance (right figure)^{26a, 26b}

One method to tackle this issue is via bandgap engineering. One example is the tantalum oxide system. Ta₂O₅ has Ta5d orbitals (which make up the conduction band) and O2p orbitals (which make up the valence band) which straddle the redox potential of hydrogen and oxygen evolution, respectively. However, its bandgap of 3.9 eV preclude visible light absorption. The nitride form Ta₃N₅, has N2p orbitals substituting the O2p orbitals leading to a decreased bandgap of 2.1 eV and near-ideal band-edge positions. The poor stability of Ta₃N₅ in aqueous environment, however, limits use as a photoanode for water oxidation. The poor electronic properties further limit the quantum efficiency for carrier collection and the quasi-Fermi level splitting (and hence photovoltage generated by a photoelectrode). Possible routes to overcome these shortcomings are by improving the surface catalytic activity of Ta₃N₅²⁵, or by forming the oxynitride phase TaON.

PEC White Paper Appendix on Energetic Mismatch

TaON combines light absorption in the visible range with photochemical stability (see Figures 1a and 1b). O2p and N2p orbitals hybridize to form the valence band.

β -TaON has shown photocatalytic activity with quantum efficiency up to 76% (for 400 nm photons) and current density greater than 3.5 mA/cm² at 0.6 V vs. Ag/AgCl^{26c}. Despite these promising results, the synthesis of β -TaON is non-trivial, and performance-limiting bulk and surface defects are yet to be identified and addressed. The photovoltage obtained from photoelectrodes is not sufficient for overall water splitting, and overall water splitting required an additional applied bias of 0.6 to 1 V, despite the large band-gap.

Another method to circumvent the energetic mismatch issue is to apply a bias in addition to the photovoltage generated by the photoelectrode. A solar cell (or multi-junction device) placed underneath the photocatalytic material can provide such bias, allowing hydrogen production from renewable solar energy only.⁶⁻⁸ The bias, in essence, “makes up” the energetic mismatch and thus enables the counter electrode to drive the reaction that does not match with the band edge level. In other words, for semiconductors whose band edge positions limit the attainable photovoltage to less than 1.23 V, additional voltage can be applied externally so that the total voltage exceeds 1.23 V. For example, n-TiO₂ has a conduction band edge that is a few hundred mV below the hydrogen evolution potential. The maximum possible photovoltage such a photoanode can generate is the energy difference between the photochemical redox reaction driven at the surface (for n-TiO₂ this is the oxygen evolution reaction) and the flat band position (which is near the conduction band edge for moderately n-doped samples). If this difference is less 1.23 eV, that photoelectrode is incapable of splitting water alone, regardless of the band gap.

The monolithic *p*-GaInP₂/*n/p*-GaAs photoelectrochemical-photovoltaic tandem cell device is a classic example of a photoelectrode biased by an underlying photovoltaic device.⁸ The device, consisting of a top *p*-GaInP₂ layer connected in series to an *n/p* GaAs bottom cell on a GaAs substrate, showed a 12.4% solar-to-hydrogen (STH) conversion efficiency with 24 h lifetime.

Alternatively, monolithic devices can be based on a photoanode biased with an integrated *p-n* junction.⁹ Another approach consists of an *n-n* heterojunction PEC device in which a photoanode is deposited onto an *n*-type semiconductor that boosts the energy of the electrons.⁹⁻¹²

Dye-sensitized nanocrystalline-nanoporous solar cell (Grätzel cell) could act as similar function. A light-to-hydrogen conversion efficiency of 4.5% was reported from the configuration combined with a nanostructured WO₃ photoanode.¹

The energy for spontaneous water splitting can also be provided by combining two photoelectrodes in series, one *n*-type and one *p*-type. Nozik in his earlier work used single crystals of *n*-TiO₂ and *p*-GaP as photoelectrodes and bonded them together through the ohmic contacts.^{13,14} NREL recently reported the performance of individual photoelectrodes connected together in the outside circuit.¹⁵ This combination relaxes the criteria governing the band edge positions. The dual-electrode configuration separates OER to the *n*- and HER to the *p*-type photoelectrodes, respectively, increasing the number of candidate semiconductors that could be used to build a stand-alone solar water splitting device.^{15,16} The key concept is that each photoelectrode generates a photovoltage given (in the ideal case where bulk recombination is minimized) by the difference from the flat band potential and the redox couple of interest. The sum of the two photovoltage must exceed 1.23 V in order for water splitting to occur. Therefore

PEC White Paper Appendix on Energetic Mismatch

to maximize the photovoltage generated by a n-type photoanode, the band edges should be raised (i.e. flat band very negative on the electrochemical scale) as high as possible. To maximize the photovoltage from a p-type photoelectrode the band edges should be lowered (flat-band potential very positive on the electrochemical scale).

In order to achieve the ideal photovoltages dictated by the band edge positions, however, requires high-quality semiconductor materials with sufficient diffusion lengths to minimize the degradation of the photovoltage due to bulk recombination. The ideal photovoltage for any semiconductor is roughly 300-400 mV less than the band-gap, but is rarely achieved due to non-ideal band edge alignment, bulk recombination, or both.

In a conceptually related approach, Domen and co-workers developed Z-scheme systems with two photocatalysts and redox couple (mediator).¹⁷⁻¹⁹ The key challenge with the redox Z-scheme is preventing internal shunting through the conducting redox mediator. Lewis and co-workers have developed p-doped Si microwires^{20,21} and are working to incorporate them with n-doped photoanodes in a tandem cell ion-conducting-membrane-supported tandem photoelectrode.²² The common point in these multiple photo-absorber approaches is that two or more photons are required to generate one electron in the external circuit. Such approaches would allow the use of lower energy photons that are unused in single semiconductor configurations.

Other strategies to improve the band edge alignment is via modifications of the semiconductor surface, either with a pH-insensitive group, producing a surface dipole that is independent of pH, or by introducing a desired surface dipole/charge.²³ Another possible way to shift the band edge up would be via quantum confinement, although this also increases the band-gap.²⁴ A 0.3-0.6 eV CB shift due to the quantum confinement effect could potentially locate the CB of hematite above the HER level, although bulk recombination issues would still remain that would likely limit the photovoltage output.

References

1. M. Grätzel, *Nature*, **414**, 338 (2001).
2. T. Bak, J. Nowotny, M. Rekas, C.C. Sorell, *Int. J. Hydrogen Energy* **27**, 991 (2002).
3. R. van de Krol, Y. Liang and J. Schoonman, *J. Mater. Chem.* **18**, 2311 (2008).
- 3b. Kumar, A.; Santangelo, P. G.; Lewis, N. S. *J. Phys. Chem.* **1992**, 96, 834-842.
4. A. Kudo and Y. Miseki, *Chem. Soc. Rev.* **38**, 253 (2009)
5. A. J. Bard and M. A. Fox, *Acc. Chem. Res.*, **28**, 141 (1995).
6. E. L. Miller, R. E. Rocheleau, X. M. Deng, *Int. J. Hydrogen Energy*, **28**, 615 (2003).
7. E. L. Miller, D. Paluselli, B. Marsen, R. E. Rocheleau, *Solar Energy Mat. Solar Cells*, **88**, 131 (2005).
8. O. Khaselev and J. A. Turner, *Science*, **280**, 425 (1998).
9. R. van de Krol, M. Grätzel; "Photoelectrochemical hydrogen production", Springer (2012)
10. R. Saito, Y. Miseki, K. Sayama; *Chem. Commun.*, **48**, 3833 (2012).
11. J. Su, L. Guo, N. Bao, C.A. Grimes; *Nano Lett.* **11**, 1928 (2011).
12. K. Sivula, F. Le Formal and M. Grätzel, *Chem. Mater.* **21**, 2862 (2009).
13. A. J. Nozik, *Appl. Phys. Lett.*, **30**, 567 (1977).

PEC White Paper Appendix on Energetic Mismatch

14. A. J. Nozik, *Phil. Trans. R. Soc. Lond. A*, **295**, 453 (1980).
15. H. Wang, T. Deutsch and J. A. Turner, *J. Electrochem. Soc.*, **155**, F91 (2008).
16. H. Wang and J. A. Turner, *J. Electrochem. Soc.*, **157**, F173 (2010).
17. R. Abe, T. Takata, H. Sugihara and K. Domen, *Chem. Commun.* 3829 (2005).
18. K. Maeda and K. Domen, *J. Phys. Chem. Lett.*, **1**, 2655 (2010)
19. K. Maeda, M. Higashi, D. Liu, R. Abe and K. Domen, *J. Am. Chem. Soc.*, **132**, 5858 (2010)
20. J.R. Maiolo III, B.M. Kayes, M.A. Filler, M.C. Putnam, M.D. Kelzenberg, H.A. Atwater, N.S. Lewis, *J. Am. Chem. Soc.* 129, 12346 (2007)
21. S.W. Boettcher, J.M. Spurgeon, M.C. Putnam, E.L. Warren, D.B. Turner-Evans, M.D. Kelzenberg, J. R. Maiolo, H.A. Atwater, N.S. Lewis, *Science* 327, 185(2010)
22. E.L. Warren, S. W. Boettcher, J.R. McKone, N.S. Lewis, *Proceedings of SPIE Volume 7770: Solar Hydrogen and Nanotechnology V*, H. Idriss and H. Wang eds. 77701F, (2010).
23. M. G. Walter, E. L. Warren, J. R. McKone, S. W. Boettcher, Q. X. Mi, E. A. Santori and N. S. Lewis, *Chem. Rev.*, **110**, 6446 (2010).
24. L. Vayssieres, C. Sathe, S.M. Butorin, D.K. Shuh, J. Nordgren, J.H. Guo, J. H., *Adv. Mater.* **17**, 2320 (2005).
25. Y. Li , T. Takata , D. Cha , K. Takanabe , T. Minegishi, J. Kubota, K. Domen; *Adv. Mater.* 2012
- 26a, 26b, 26c. Domen et al., *J. Phys. Chem. B*, 107 (2003) 1798; *Catal. Today* 78 (2003) 555; *J. Am. Chem. Soc.*, 2010, 132 (34)

PEC White Paper Appendix: Theoretical Studies

Design and Characterization of Photoelectrodes from First Principles

Team	Affiliation	Task
Tadashi Ogitsu Brandon Wood Wooni Choi	Lawrence Livermore National Laboratory	Photocatalysts-electrolyte interface
Muhammad N. Huda	University of Texas at Arlington	Novel photo-catalytic materials design
Su-Huai Wei	National Renewable Energy Laboratory	Corrosion mitigation strategy

Although significant performance improvements have been realized since the first demonstration of sunlight-driven water splitting in 1972, mainstream adoption of photoelectrochemical (PEC) cells remains limited by an absence of cost-effective electrodes that show simultaneously high conversion efficiency and good durability. Here we outline current and future efforts to use advanced theoretical techniques to guide the development of a durable, high-performance PEC electrode material. Working in close collaboration with experimental synthesis and characterization teams, we use a twofold approach focusing on: 1) rational design of novel high-performance electrode materials by methods beyond traditional band-engineering; and 2) characterization and optimization of the electrode-electrolyte interface.

Introduction

A photoelectrochemical (PEC) hydrogen production device uses sunlight and water to generate hydrogen gas with no adverse emissions, and as such is considered an ideal sustainable energy solution. Since the first successful demonstration of hydrogen production from sunlight and water using a TiO_2 photoelectrode in 1972,² steady improvement on solar-to-hydrogen (STH) efficiency has been made. For instance, in 1997-1998, a silicon triple-junction solar harvester combined with cobalt-based co-catalyst resulted in a STH efficiency of about 8%.^{3,4} In 1998, the current record STH efficiency of 12.4% was established at NREL using a $\text{GaInP}_2/\text{GaAs}$ tandem cell with a Pt co-catalyst.⁵

Despite these breakthroughs, the PEC research community has faced great challenges in achieving high STH and durability simultaneously, which has impeded commercial use of PEC technology. Since no known material currently satisfies established U. S. Department of Energy target windows that would lead to widespread market adoption,⁶⁻¹² it is highly desirable to devise a targeted, rational approach for developing entirely new photoelectrode materials and/or surface modifications. This has proven challenging, in part because it is not fundamentally understood how the interplay between the various electrode materials properties impacts the overall device

PEC White Paper Appendix: Theoretical Studies

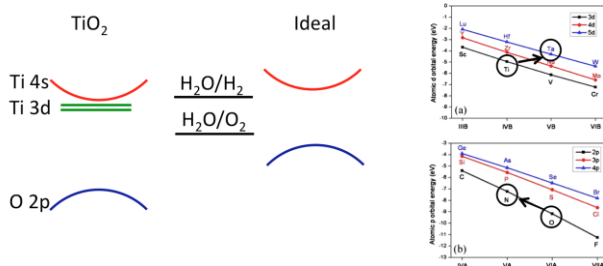


Figure 1: Cartoon images describing one possible strategy for improving TiO_2 electrode properties.¹ From left to right: Schematic electronic structure of TiO_2 ;⁶⁾ $\text{H}_2\text{O}/\text{H}_2$ and $\text{H}_2\text{O}/\text{O}_2$ water redox potentials; schematic band structure of an ideal PEC electrode; plots on levels of atomic orbitals (from ref [23]). TiO_2 has a conduction band (CB) that is too low with respect to the water redox potentials and possesses localized character owing to the Ti 3d states; similarly, the O 2p-derived valence band (VB) is too low and localized. An ideal material should have CB and VB edges straddling the $\text{H}_2\text{O}/\text{O}_2$ redox potentials so as to overcome any electron-transfer reaction barriers with minimal energy loss, and possessing delocalized character to ensure good carrier transport. The right-hand plot shows that one can rationally substitute atoms in order to improve the band alignment and the transport, for instance by substituting Ti with Ta (or W) and O with N.¹

to achieve improved performance. The understanding provided by these studies has led to consistent modification of PEC material design strategies over the last decade (see Fig. 1).^{1, 13-33}

A second challenging aspect of this problem is the lack of information on the microscopic properties of electrode-electrolyte interface. When the electrode is immersed in electrolyte (even without illumination), the surface becomes contaminated by foreign chemical species. When the electrode is illuminated, the situation becomes even more complex. In addition to hydrogen and oxygen evolution, various additional types of chemical reactions, including photocorrosion, can be driven at the electrode-electrolyte interface by photogenerated carriers. Without detailed information on the microscopic structure and chemistry of the interface, formulating a consistent strategy to optimize interfacial properties becomes extremely difficult, if not impossible. In order to better understand the active interfacial processes, we have begun performing large-scale first-principles molecular dynamics simulations to examine the structure and reactivity of realistic electrode-electrolyte interfaces (see Fig 2).²⁹⁻³³

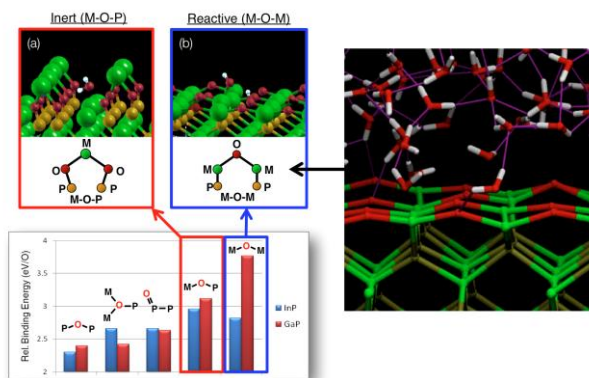


Figure 2: It was demonstrated that the local bonding topologies of an oxidized III-V surface are a descriptor of chemical activity (left). This local model approach was successfully applied to rationalize the chemical activities observed in the direct first-principles molecular dynamics simulations of the water/III-V interface (right). From ECS presentation, Boston (2011) by Wood, Schwegler, and Ogitsu.

Such simulations have become possible only in recent years, thanks to significant advances in supercomputer performance and novel software algorithms

performance. In this regard, advanced theoretical techniques are ideally suited for offering a detailed description of the underlying properties, and as such could be an extremely valuable tool for intelligently guiding future design efforts.

In practice, many of the materials properties that directly impact solar harvesting efficiency, corrosion resistance, and catalytic activity appear to be correlated. As a result, optimizing one property (e.g., STH efficiency) frequently compromises another (e.g., durability). One of the challenges has been to understand the nature of this correlation in the bulk electrode materials, and whether key properties can be simultaneously optimized in real devices. Accordingly, our first approach focuses on the use of first-principles density functional theory (DFT) calculations to investigate mechanisms for independently improving intrinsic semiconductor properties

PEC White Paper Appendix: Theoretical Studies

To summarize, our theory effort focuses on two areas: electrode material design and characterization of interfacial properties. Dr. Huda at UTA will refine and deploy the materials design strategies by innovative mineral database search algorithm and calculate the materials' electronic and optical properties at both crystalline and nano-crystalline phases. The LLNL team will continue their theoretical studies on the semiconductor-electrolyte interface using first-principles molecular dynamics simulations. Their focus will be on investigating surface stabilization and activation mechanisms based on modification of the interfacial structure and chemistry. Dr. Wei at NREL will develop corrosion mitigation strategy based on modification of activation potentials of oxidation and reduction reactions. In all cases, information obtained from these activities will be shared with the collaborators on the materials synthesis and characterization teams, as well as the wider PEC research community, in order to accelerate the development of a viable PEC electrode material.

Task I: Rational Design of Electrode Materials

(Task lead by Huda at UTA)

Focus: Theoretically/computationally design of novel crystalline and nano-crystalline photocatalyst materials and their simultaneous optimization of electronic, optical, and transport properties.

A general scheme to predictively tune materials band structure properties are following: (1) By isovalent doping, (2) by passivated co-doping, (3) By predicting novel alloys, and (4) By modifying the shape and size of the materials, e.g., by forming nanostructures.

Our proposed research topics mainly targeting number 3 and 4 of the above scheme:

(i) Novel photocatalysts prediction by mineral database searching: The discovery of efficient photo-catalysts is one of the grand challenges for energy conversion and storage. As naturally occurring materials do not fulfill all the required electronic criteria, these electronic requirements in materials are usually achieved by a band-engineering approach, where the electronic structures of the materials are engineered by selective doping. However, the introduction of impurities generally creates unwanted defect states in band gap, which are detrimental to the transport properties due to poor crystallinity³⁴. To-date shifting the optical absorption spectrum of a material to the visible region by doping-only process has not been successful in improving the photoconversion efficiency significantly.

Instead of following a simple band-engineering-only approach, we plan to follow a “natural selection” process. As the minerals were already formed in earth over millions of years, they clearly possess thermodynamic stability, and represent ideal candidates to design materials for energy-related applications. Though these naturally occurring minerals by themselves may not be directly suitable for energy conversion, the knowledge of chemical compositions of these minerals may lead to a proper photo-conversion material. Their compositions and properties can easily be determined by theory calculations, and, instead of doping, a new alloy based on the selected mineral will be predicted. Once predicted by theory, these existing but untested structures then can be evaluated experimentally for photocatalysis. In this proposed research, we will also develop an efficient selection algorithm for mineral database search.

(ii) Nano-crystalline photocatalysts: The current understanding at the “nano” level of oxides is not very clear, and leads to misleading assumptions to the photocatalytic potential of

PEC White Paper Appendix: Theoretical Studies

nano-crystals. Thus understanding of size- and shape-induced effects is crucial for efficient design of metal-oxide nano-crystalline photocatalysts. First principle theories, such as DFT and time-dependent-DFT (TDDFT), are state of the art theoretical methods to shed light in these aspects. Several key issues remain challenging in metal-oxide nano-crystals so far; some of them are: (i) identification of the fundamental gap and the actual optical gap, (ii) the nature of energy levels (“band”) in the nano-crystals, (iii) the effects of surface and surface passivation, (iv) the difference between the flat band potential (surface) and the band position in the “bulk” of nano-crystals, (v) transport of charge carriers after photo-excitation, and (vi) extraction or injection of electrons from or to the nano-crystals’ surface.

We have recently shown that a unique set of self-passivated and charge compensated delafossite nanocrystals can be highly stable with some interesting optical properties. These behavior needs to be explored in other metal oxides nanocrystals with various sizes and shapes as well.

Task II: Characterization and Optimization of the Electrode-electrolyte Interface

(Task lead by Ogitsu at LLNL)

Focus: Gain atomistic insight into the properties of electrode-electrolyte interface in order to develop a corrosion mitigation strategy and to improve STH conversion efficiency.

LLNL’s plan initially involves investigation of the GaInP₂ (001) surface both with and without an electrolyte. This will be done in order to understand which microscopic interfacial properties are necessary to achieve high STH, and how these are affected by the presence of an electrolyte. We will then simulate and compare the in-situ XAS/XES data for our model systems with experimental results from the UNLV surface characterization team, which will allow us to verify which of our proposed atomistic mechanisms are indeed related to hydrogen evolution and corrosion. Simulation results will be compared with data from NREL’s recent attempts at surface stabilization via nitrogen treatment. In doing so, we aim to extract a mechanism for atomistic surface stabilization and to develop an improved corrosion mitigation strategy for GaInP₂. It is expected that these efforts will interface closely with and provide feedback to the rational materials design effort (Task I), particularly given that Dr. Wei is recognized as one of the leading experts on GaInP₂.³⁵⁻³⁸

i) Simulation of the GaInP₂(001)-water interface: The first subtask involves the application of previously established static and dynamic methods for GaP(001) and InP(001) to the alloy material GaInP₂(001). In addition to extracting structural motifs that can be used in subsequent models, we will assess the role of alloy structure on the chemical properties of the interface. Simulations will be done with and without additional surface contaminants.

ii) Investigation of substitutional impurities: In FY12, T. Deutsch *et al.* (NREL) discovered that a specific type of nitrogen incorporation to GaInP₂ electrode may improve the durability significantly with an acceptably minimal impact on STH efficiency. For our second subtask, we intend to investigate in detail the effect of nitrogen doping on surface corrosion resistance in order to gain microscopic insight on the atomistic surface stabilization mechanism.

PEC White Paper Appendix: Theoretical Studies

iii) Simulation of XAS/XES spectra: For our third subtask, we plan to simulate X-ray absorption (XAS) and emission (XES) spectra of reference model surfaces. These will be done on clean surfaces, as well as oxygen- and hydroxyl-contaminated surfaces, which are better approximations to the electrode structure when immersed in electrolyte. The goal of this stage is to establish and validate accurate models for the precursory interfacial structure present prior to illumination. For this part of research activity, the LLNL team is collaborating with Dr. Prendergast at LBNL (Computational Spectroscopy Group of The Molecular Foundry). Notably, optimized computational procedures for simulating the P-L_{2,3} edge XAS/XES of GaInP₂ have already been established and tested.

iv) Surface oxide modeling: Experimental characterization of actual GaInP₂ electrodes by the UNLV team found a >1nm native oxide on the surface. If resources permit, we will develop and investigate indium/gallium oxide-water interface models, including the generation of corresponding computational spectra to compare with the UNLV/NREL results. These could be particularly useful for detailing the atomistic corrosion mechanism, as well as its relationship with the hydrogen evolution mechanism. An initial comparison of the experimental data with our current models should allow us to better assess the necessity of these additional spectra. If necessary, we will revise our model structures until we come to a satisfactory agreement between experiment and theory.

Task III: Corrosion Mitigation Strategy

(Task lead by Wei at NREL)

Focus: Investigate on energy barrier of oxidation reaction, and develop corrosion mitigation strategy

The photocorrosion in semiconductor is mainly due to photo generated holes which oxidize the semiconductor or photo generated electrons that reduce the semiconductor. In order to improve the durability we have to either migrate the photo generated holes or electrons to other materials, which are stable for water splitting, or find semiconductors with chemical potentials of all semiconductor oxidation reactions below the water oxidation potential and chemical potentials of all semiconductor reduction reactions above the water reduction potential, so the photo generated holes and electrons will relax to water oxidation and reduction levels, thus driving the water splitting reactions instead of driving the semiconductor reactions. For example, we calculated the electron potential of GaP reduction reaction and hole potential of GaP oxidation reaction as shown in Fig. 7. The GaP reduction potential is found to be above the water reduction potential and thus photo generated electron will most likely drive the H₂O/H₂ reaction. The GaP oxidation potential is, however, above the water oxidation potential and thus hole will most likely drive the GaP oxidation instead of O₂/H₂O reaction. If we can engineer the GaP surface to create an energy barrier larger than the energy difference between GaP oxidation and water oxidation potentials to block the GaP oxidation reaction, then we may be able to significantly improve the durability of GaP as water splitting photocatalysts.

PEC White Paper Appendix: Theoretical Studies

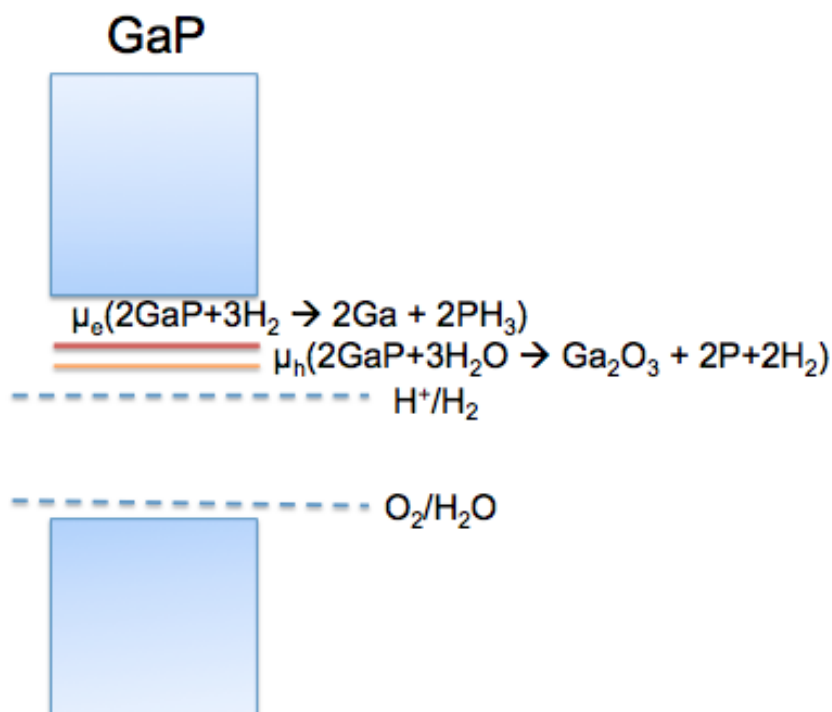


Figure 3: Band alignment of GaP with respect to water redox potentials as well as the electron potential of GaP reduction reaction and hole potential of GaP oxidation reaction.

Summary

In summary, we have outlined a twofold approach that uses advanced theoretical techniques to develop design and optimization strategies for efficient, durable PEC photoelectrodes. First, we use first-principles density functional theory calculations to successfully predict novel photocatalyst materials of new composition by an intelligent search of the mineral database and assess their electronic, optical, and transport properties at both crystalline and nano-crystalline phase for further screening. Second, we use first-principles molecular dynamics simulations and model free-energy reaction barrier calculations to examine the structure and chemistry of the surface, with the goal of improving device stability and performance. Third, based on the free-energy reaction barrier calculations, we will develop corrosion mitigation strategy. Together with the efforts of other members of the DOE/EERE Photoelectrochemical Hydrogen Production Working Group, the theory team's input should provide much-needed insight into how specific photoelectrode materials properties should be combined so as to engineer and optimize devices that meet the DOE market adoption targets.

References

- ¹ W.-J. Yin, H. Tang, S.-H. Wei, M. M. Al-Jassim, J. Turner, and Y. Yan, *Phys Rev B* **82** (2010).
- ² A. Fujishima and K. Honda, *Nature* **238**, 37 (1972).

PEC White Paper Appendix: Theoretical Studies

- 3 R. E. Rocheleau and E. L. Miller, *Int J Hydrogen Energ* **22**, 771 (1997).
- 4 R. E. Rocheleau, E. L. Miller, and A. Misra, *Energy & Fuels* **12**, 3 (1998).
- 5 O. Khaselev and J. A. Turner, *Science* **280**, 425 (1998).
- 6 "*Hydrogen and Fuel Cells Program Plan*", (Department of Energy, Washington D.C., 2011)
- 7 "*Fuel Cell Technologies Program Multi-Year Research, Development and Demonstration Plan: 3.1 Hydrogen Production, 2011 Interim Update*", (Department of Energy, Washington D.C., 2011)
- 8 "*Basic Research Needs for Solar Energy Utilization*", (Department of Energy, Washington D.C., 2005)
- 9 "*Hydrogen Posture Plan*", (Department of Energy, Washington D.C., 2006)
- 10 "*Basic Research Needs for the Hydrogen Economy*", (Department of Energy, Washington D.C., 2004)
- 11 "*National Hydrogen Energy Roadmap*", (Department of Energy, Washington D.C., 2002)
- 12 "*A National Vision of America's Transition to a Hydrogen Economy -- To 2030 and Beyond*", (Department of Energy, Washington D.C., 2002)
- 13 A. Walsh, J. L. F. Da Silva, Y. Yan, M. M. Al-Jassim, and S.-H. Wei, *Phys Rev B* **79** (2009).
- 14 A. Walsh, et al., *Energ Environ Sci* **2**, 774 (2009).
- 15 A. Walsh, Y. Yan, M. M. Al-Jassim, and S.-H. Wei, *Journal of Physical Chemistry C* **112**, 12044 (2008).
- 16 A. Walsh, Y. Yan, M. N. Huda, M. M. Al-Jassim, and S.-H. Wei, *Chem Mater* **21**, 547 (2009).
- 17 M. N. Huda, Y. F. Yan, S. H. Wei, and M. M. Al-Jassim, *Phys Rev B* **78** (2008).
- 18 M. N. Huda, Y. Yan, A. Walsh, S.-H. Wei, and M. M. Al-Jassim, *Appl Phys Lett* **94** (2009).
- 19 M. N. Huda, Y. Yan, A. Walsh, S.-H. Wei, and M. M. Al-Jassim, *Phys Rev B* **80** (2009).
- 20 M. N. Huda, Y. Yan, C.-Y. Moon, S.-H. Wei, and M. M. Al-Jassim, *Phys Rev B* **77** (2008).
- 21 W.-J. Yin, S.-H. Wei, M. M. Al-Jassim, and Y. Yan, *Phys Rev Lett* **106** (2011).
- 22 W.-J. Yin, S.-H. Wei, M. M. Al-Jassim, and Y. Yan, *Appl Phys Lett* **99** (2011).
- 23 W.-J. Yin, S.-H. Wei, M. M. Al-Jassim, J. Turner, and Y. Yan, *Phys Rev B* **83** (2011).
- 24 M. N. Huda, Y. Yan, A. Walsh, S.-H. Wei, J. A. Turner, and M. M. Al-Jassim, in *Solar Hydrogen and Nanotechnology V*, edited by H. W. H. Idriss, 2010), Vol. 7770.
- 25 M. N. Huda, A. Walsh, Y. Yan, S.-H. Wei, and M. M. Al-Jassim, *J Appl Phys* **107** (2010).
- 26 C. Feng, W.-J. Yin, J. Nie, X. Zu, M. N. Huda, S.-H. Wei, M. M. Al-Jassim, J. A. Turner, and Y. Yan, *Appl Phys Lett* **100** (2012).
- 27 Y. Gai, J. Li, S.-S. Li, J.-B. Xia, and S.-H. Wei, *Phys Rev Lett* **102**, 036402 (2009).
- 28 W.-J. Yin, S. Chen, J.-H. Yang, X.-G. Gong, Y. Yan, and S.-H. Wei, *Appl Phys Lett* **96**, 221901 (2010).
- 29 "*Characterization and Optimization of Photoelectrode Surfaces for Solar-to-Chemical Fuel Conversion*", (Department of Energy, Washington D.C., 2010)
- 30 B. Wood, T. Ogitsu, and E. Schwegler, in *SPIE Optics + Photonics 2010* (SPIE, San Diego, 2010).
- 31 B. C. Wood, T. Ogitsu, and E. Schwegler, *Journal of Photonics for Energy* **1**, 016002 (2011).
- 32 B. C. Wood, T. Ogitsu, and E. Schwegler, *The Journal of Chemical Physics* **136**, 064705 (2012).

PEC White Paper Appendix: Theoretical Studies

- 33 "Characterization and Optimization of Photoelectrode Surfaces for Solar-to-Chemical Fuel
Conversion", (Department of Energy, 2011)
- 34 K.-S. Ahn, Y. Yan, and M. Al-Jassim, Journal of Vacuum Science & Technology B:
Microelectronics and Nanometer Structures **25**, L23 (2007).
- 35 S. H. Wei and A. Zunger, Appl Phys Lett **56**, 662 (1990).
- 36 S.-H. Wei and A. Zunger, Phys Rev B **57**, 8983 (1998).
- 37 A. Franceschetti, S.-H. Wei, and A. Zunger, Phys Rev B **52**, 13992 (1995).
- 38 S.-H. Wei, D. B. Laks, and A. Zunger, Appl Phys Lett **62**, 1937 (1993).